

# Enceladus

**M. L. Cable**

*NASA Jet Propulsion Laboratory*

**M. Neveu**

*NASA Goddard Space Flight Center/University of Maryland, College Park*

**H.-W. Hsu**

*University of Colorado*

**T. M. Hoehler**

*NASA Ames Research Center*

---

Enceladus has recently come into the spotlight as one of the key targets for astrobiology exploration in the solar system. Discoveries that arose from data returned by the Voyager and Cassini spacecrafts from this tiny, intriguing moon provide tantalizing evidence of a global, subsurface ocean with water-rock interaction at its base, accessible via a sustained plume ejected from fissures at the south pole. Based on current understanding, the ocean of Enceladus is habitable. The next logical question to investigate is, does it have life? In this chapter we review the evidence for Enceladus' ocean and its habitability, identify constraints and outstanding questions on the extent of the supply of life's key ingredients, discuss how this supply might constrain the detectability of any life in Enceladus' interior, and present strategies to search for life in the specific context of Enceladus in the coming decades.

*Life is flux.*

— *Heraclitus (ca. 535–ca. 475 BCE)*

## 1. INTRODUCTION

Enceladus, a small moon in orbit around Saturn, has been full of surprises since it was first identified in 1789. The discovery of Enceladus is credited in part to William Herschel, who was fortuitously observing Saturn at equinox. During equinox, the Sun and Earth are aligned edge-on with the rings of Saturn, reducing the observed reflection of sunlight off the rings (ringshine), which is usually bright enough to mask Enceladus from most telescopes. Enceladus is named after one of the Titans, giants in Greek mythology, and contrary to its small size (504 km or 313 miles in diameter), it has lived up to this legacy.

Enceladus is a particularly exciting target for astrobiology in the solar system because it appears to be active and accessible: A recently discovered persistent water plume emanating from fissures near its south pole can provide a direct link to its global subsurface ocean. This ocean appears to meet the criteria for a habitable environment: extended regions of liquid water, conditions favorable for the assembly of complex organic molecules, and energy source(s) to sustain putative metabolism (*Des Marais et al.*, 2008). If these habitable conditions were present for an extended period over

Enceladus' history, the ocean could have supported life in the past, or might even host life today. Ocean material ejected from Enceladus through the plume eventually orbits Saturn as one of its outermost rings, the E ring.

The record of *in situ* observations of Enceladus spans decades. Given Enceladus' location within the E ring of Saturn and that the maximum intensity of this ring occurs near the orbit of Enceladus, it had been hypothesized from Voyager 1 observations that Enceladus was the primary source for E-ring particles (*Stone and Miner*, 1981). The orbital mean-motion resonance of Enceladus with another saturnian moon, Dione (a configuration that can promote noncircular orbits and therefore enhance tidal dissipation heating), led some to guess, even then, that these particles may be formed due to outgassing of liquid water from under a thin crust (*Terrile and Cook*, 1981). No backlit images of the Saturn system were obtained by Voyager 2 due to a malfunction of the scan platform (*Marchetto*, 1983); if it had not jammed, it is possible that Voyager 2 might have captured the first images of the Enceladus plume. Instead, confirmation of the plume, the connection between Enceladus and the E ring, and the presence of a global, subsurface ocean would require a dedicated mission to the Saturn system: Cassini-Huygens. [We note

that recently a post-processed image taken by Voyager 1 appears to show a faint outline of the Enceladus plume (Stryk, 2017). However, as this image processing was not possible until recently, the Cassini-Huygens mission is still credited with discovery of the Enceladus plume.]

The Cassini-Huygens mission completely revolutionized our understanding of the saturnian system, with Enceladus as a prime example. The discovery of Enceladus' plume (Porco *et al.*, 2006; Dougherty *et al.*, 2006; Hansen *et al.*, 2006; Spahn *et al.*, 2006; Tokar *et al.*, 2006; Waite *et al.*, 2006) and its source — over 100 jets located along four surface fissures called “tiger stripes” in the south polar terrain (SPT) — provided strong evidence for a subsurface liquid water reservoir (Schmidt *et al.*, 2008; Postberg *et al.*, 2009, 2011). This reservoir is not a local sea but a global ocean, as demonstrated by two independent lines of evidence (Hemingway and Mittal, 2019). First, interpretation of gravity measurements (McKinnon, 2015; Čadek *et al.*, 2016; Beuthe *et al.*, 2016) suggests that the rapid (33-hr) spin of Enceladus affects the depth below which all pressures are hydrostatic (only due to gravity). The simplest explanation for this is a floating ice shell of variable thickness (Airy isostasy) sitting on top of a global ocean. Second, careful analysis of Enceladus images collected over seven years of Cassini observations revealed that Enceladus' rotation has a forced physical libration (wobble), too large to be consistent with a crust grounded to the core (Thomas *et al.*, 2016). Again, the simplest explanation is a free-floating crust, which is only possible if there is a global ocean.

The implication of a global ocean as opposed to a regional sea is important for life because unlike a regional sea, a global ocean likely persists long enough for a biosphere to emerge [this took <1 b.y. on Earth (e.g., Dodd *et al.*, 2017)]. A regional sea could have been formed by an impact and might only last millions of years (Roberts and Stickle, 2017). In contrast, a global ocean requires heating rates that on a small moon like Enceladus can only be generated by the dissipation of tides raised by a large body like Saturn. Tidal dissipation can be caused by orbital eccentricity (i.e., a noncircular orbit) driven by gravitational interactions with other moons in the saturnian system. Via this mechanism, tidal dissipation may take several hundred million years to subside, even once the orbital forcing ceases [the orbital circularization timescale (e.g., Henning and Huford, 2014; Choblet *et al.*, 2017)]. Enceladus' orbit is currently forced to be eccentric due to interactions with Dione. The corresponding dissipation was thought to be too small to account for the high heat fluxes determined from Cassini measurements (Meyer and Wisdom, 2007; Choblet *et al.*, 2017). However, Enceladus' orbit was recently found to expand at a surprisingly fast rate (Lainey *et al.*, 2017), indicating that Saturn's tidal torque on Enceladus is higher than expected. This torque is likely able to transfer energy from Saturn's spin into heat inside Enceladus quickly enough to maintain the current ocean (Nimmo *et al.*, 2018). Tidal dissipation could also have been higher in the geologically recent past (Neveu and Rhoden, 2019). In any case, with a global subsurface

ocean, Enceladus beckons as one of the few places in the solar system where suitable conditions may have existed long enough for life to gain a foothold (Fig. 1). Because material exchange with the inner solar system is unlikely (Worth *et al.*, 2013), any life on Enceladus would likely have emerged independently of life on Earth, and therefore would have much to teach us about which features of life are universal.

Enceladus might hold the key for discovering life in our own cosmic backyard, and it has provided a facile means to access it via the plume. With nearly 25 yr of observations of the E ring from the Voyager era (Haff *et al.*, 1983), over 10 yr of direct observation of the plume by Cassini, and models that suggest that the plume is modulated by tidal dissipation (Hedman *et al.*, 2013; Běhouňková *et al.*, 2015; Pathhoff and Kattenhorn, 2011), we know that the plume is a long-lived phenomenon lasting at least tens to hundreds of years (section 2.4). This makes Enceladus the only confirmed place in the solar system where we can sample fresh material from the subsurface ocean without the need to dig or drill. [Europa may also have a plume (see Sparks *et al.*, 2017; Jia *et al.*, 2018; Arnold *et al.*, 2019; and references therein; see also the chapter by Schmidt in this volume); the plumes of Neptune's moon Triton have not been conclusively linked to a subsurface ocean source (see Kirk *et al.*, 1995).]

In this chapter, we address the astrobiological relevance of Enceladus from the outside-in. Section 2 describes the plume composition and structure. We address how this plume is connected to the subsurface ocean in section 3. In section 4, we delve deep into the ocean itself, and its interaction with the core. Section 5 takes these puzzle pieces and constructs a picture of Enceladus in the context of astrobiology. Finally, in section 6 we discuss how this picture informs the search for life at Enceladus: what biosignatures are most relevant, and where we might find them. However, our current picture of Enceladus is not complete; in section 7 we highlight some questions still unanswered for this fascinating moon.

## 2. PLUME COMPOSITION AND STRUCTURE

The plume of Enceladus is sourced from multiple (~100) jets and curtain eruptions located in surface hot spots along prominent parallel troughs called tiger stripes (Porco *et al.*, 2006, 2014; Spencer *et al.*, 2006; Spitale *et al.*, 2015) located in Enceladus' SPT. These emissions are likely fed by coupled freezing and vaporization of liquid water beneath the icy crust (Schmidt *et al.*, 2008; Nakajima and Ingersoll, 2016; Kite and Rubin, 2016), producing a plume that extends for thousands of kilometers and subsequently forms the E ring around Saturn (Spahn *et al.*, 2006; Kempf *et al.*, 2010; Mitchell *et al.*, 2015).

### 2.1. Plume Composition

Enceladus' plume was sampled *in situ* by the Cassini spacecraft during multiple fly-throughs over the course of the mission (Fig. 2). Measurements have revealed that the plume is primarily composed of *gas* and *grains*.

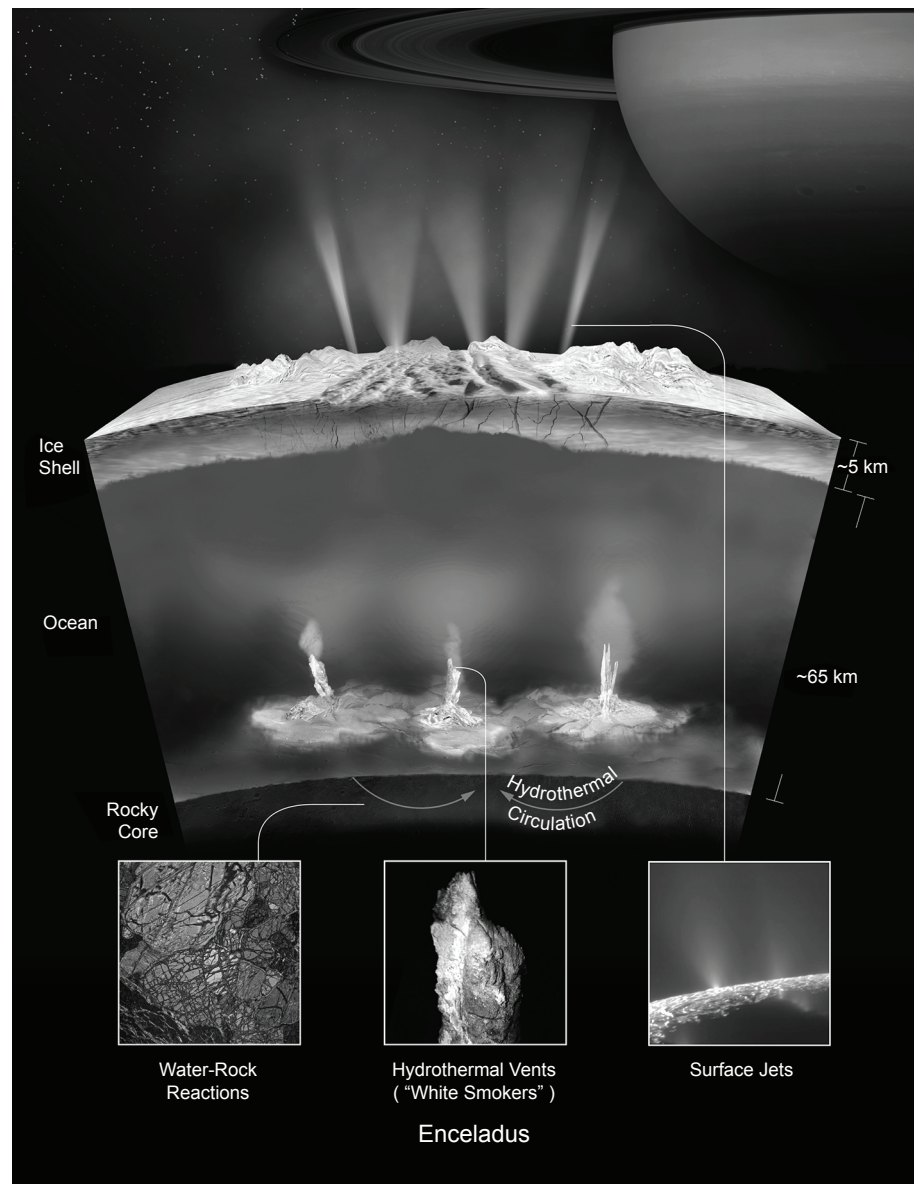


**Fig. 1.** See Plate 18 for color version. Enceladus' plume is sourced from a subsurface ocean in contact with the rocky core below at temperatures indicating hydrothermal activity. Credit: NASA/JPL-Caltech/SwRI.

The gas is mostly comprised of water vapor (Table 1), although importantly, significant amounts of methane and molecular hydrogen ( $H_2$ ) have also been detected by the Cassini Ion and Neutral Mass Spectrometer (INMS). The methane may be too abundant to be formed solely from the decomposition of clathrate hydrates (methane trapped in water cages), indicating another process is at work (Bouquet et al., 2015). This is supported by the detection of  $H_2$  in the plume, strongly suggesting that the ocean of Enceladus is in contact with, and reacting with, the rocky core through hydrothermal processes (Waite et al., 2017) (sections 3.2 and 4.3). These reactions drive the ocean out of chemical equilibrium, in a similar way to water around Earth's hydrothermal vents, potentially providing a source of chemical energy that life could exploit.

The plume grains have been detected and characterized by several instruments onboard Cassini, including the Cos-

mic Dust Analyzer (CDA) (Spahn et al., 2006; Postberg et al., 2009, 2011), the Cassini Plasma Spectrometer (CAPS) (Jones et al., 2009), the Radio and Plasma Wave Science (RPWS) instrument (Ye et al., 2014), and INMS (Teolis et al., 2010, 2017). The closest Cassini fly-through was at an altitude of 25 km, so any grains too large or heavy to be lofted to this altitude were not sampled. The grains have been categorized based on composition (Table 2): water-rich (Type I), organic- or silicate-rich (Type II), and salt-rich (Type III).

Type I grains are almost pure water ice and tend to be small (typically  $<0.6 \mu\text{m}$ ), implying that they are likely formed by homogeneous nucleation from the gas phase (Postberg et al., 2011); this is supported by models of water vapor flow and condensation rates that are consistent with Cassini data of plume brightness and particle size distribution (Schmidt et al., 2008). Salt-rich grains (Type III) tend to



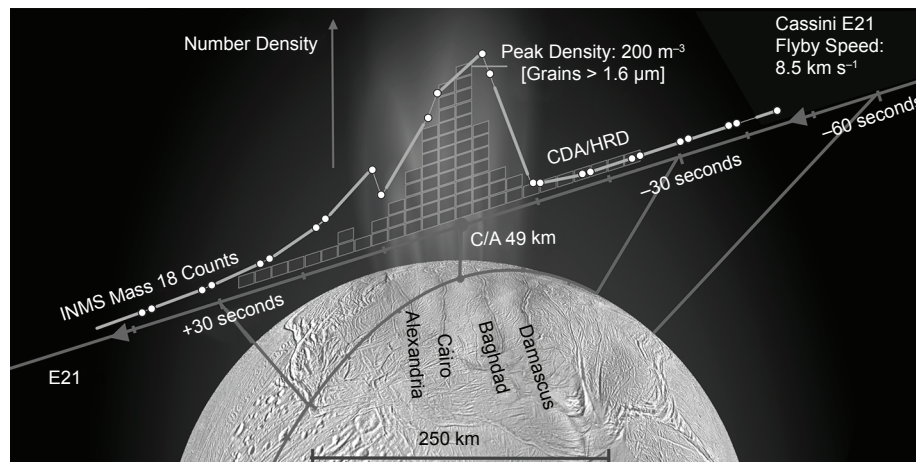


**Fig. 2.** See Plate 19 for color version. Plume ice grain and neutral gas profiles for the Cassini E21 fly-through of the Enceladus plume measured by the CDA High Rate Detector (HRD) (green boxes) and INMS (orange trace). The neutral gas profile shown is of water vapor ( $\text{H}_2\text{O}$  has a mass of 18 u). Closest approach (C/A) for this fly-through is indicated at 49 km altitude (this was the last and one of the closest plume crossings), with the time-delineated groundtrack outlined on Enceladus' surface in blue. In this image, the south pole of Enceladus is oriented up.

have 0.5–2% sodium and potassium salts by mass (Postberg *et al.*, 2011). These particles are typically larger ( $>0.6 \mu\text{m}$ ), and are probably formed from flash freezing of salt water from the ocean (Postberg *et al.*, 2009).

Type II particles contain either organic or silicate impurities. Oxygen- and nitrogen-bearing volatile organic species have been identified in both the gas (Magee and Waite, 2017) and ice grain phases (Khawaja *et al.*, 2019), which could be synthesized to form more complex organic molecules through hydrothermal processes. Interestingly, a subset of these particles (~12% of Type II grains, ~3% of all E-ring particles) contain organic molecules with masses greater than 200 u (u = unified atomic mass units; as an example, the mass of glycine, the simplest amino acid, is 75 u; see Fig. 3). These organic molecules, called high mass organic cations (HMOC), are found in high abundance (~1% by mass) in these particles, and appear to be unsaturated (containing double and triple carbon-carbon and carbon-nitrogen bonds) and partially aromatic (containing cyclic structures). Significantly, analysis of CDA and INMS spectra collected at different velocities indicate that these species are probably fragments of even larger organic molecules, as the distribution of organics detected shifted to lower masses with

increasing impact velocity (Postberg *et al.*, 2018; Waite *et al.*, 2009). However, Cassini's instruments lacked the mass range and resolution to characterize these fascinating organics any further. For more discussion of how such large, nonvolatile molecules might be expelled in the plume, see section 3.

## 2.2. Fate of the Plume Grains

The motion of grains in the plume is determined by gravity as well as other perturbing forces, whose ratio depends on the grain size. Smaller grains ( $<1 \mu\text{m}$ ) are dominated by electromagnetic forces and can accumulate electric charges via collisions as the particles pass through the vents (Jones *et al.*, 2009). These grains could be picked up by Saturn's magnetosphere (Meier *et al.*, 2014; Mitchell *et al.*, 2015) and can escape with the plume gas to form the E ring (Porco *et al.*, 2006; Kempf *et al.*, 2010). A significant fraction of the larger grains ( $\geq 1 \mu\text{m}$ ) fall back to the surface of Enceladus, covering craters and making the surface of Enceladus the whitest and most reflective in the solar system (Southworth *et al.*, 2019; Porco *et al.*, 2006, 2017; Hedman *et al.*, 2009; Kempf *et al.*, 2010; Howett *et al.*, 2010; Verbiscer *et al.*, 2007; Schenk *et al.*, 2011).

Once in the E ring, these ice grains are exposed to two important space weathering processes: sputtering erosion and plasma drag by the magnetospheric plasma ions (Jurac *et al.*, 2001; Dikarev, 1999). In addition to the effects on long-term E-ring dynamics (Horányi *et al.*, 2008), the silica ( $\text{SiO}_2$ ) nanograins detected by the CDA instrument might be released from the E-ring grains by sputtering erosion. The high abundance and specific size distribution (particle radius  $<10 \text{ nm}$ ) of these nanograins indicate the pH (8.5–10.5, moderately alkaline) and temperature ( $\geq 90^\circ\text{C}$ ) at which they formed, most likely via homogeneous nucleation (Hsu *et al.*, 2015). These tiny sputtered nanograins provided the first evidence that hydrothermal reactions are occurring below the ocean floor of Enceladus.

TABLE 1. Major species present in Enceladus' plume gas.

Constituent	Mixing Ratio (%)
$\text{H}_2\text{O}$	96 to 99
$\text{CO}_2$	0.3 to 0.8
$\text{CH}_4$	0.1 to 0.3
$\text{NH}_3$	0.4 to 1.3
$\text{H}_2$	0.4 to 1.4

Reproduced from Waite *et al.* (2017).

TABLE 2. Enceladus plume grain composition (number density) for particles  $>0.2 \mu\text{m}$  detected by CDA in the E ring or during plume fly-throughs at altitudes  $\geq 25 \text{ km}$  (Postberg et al., 2008, 2009, 2011).

Grain Type	Plume Mixing Ratio (%)	E-Ring Mixing Ratio (%)	Composition
Type I	30	$\sim 70$	Almost pure water ice (Na/H <sub>2</sub> O mixing ratio $\sim 10^{-7}$ )
Type II	$>30$	25	Either organic-rich (hydrocarbons or polar organics) or silicate-rich ( $\sim 1\%$ by mass Mg-rich, Al-poor mineral inclusions in water ice)
Type III	$<40$	6*	0.5–2% by mass Na, K salts (mostly NaCl and NaHCO <sub>3</sub> )

\*The salt-rich Type III grains tend to be larger, and so are less likely to escape Enceladus' gravity and reach the E ring.

### 2.3. Plume Structure

The structure of the plume provides essential information on the interrelationship of the water vapor and ice grains in the vents, connecting to the subsurface ocean. After emerging from the surface, micrometer-sized ice grains soon collisionally decouple from the ascending gas flow. Their motion is mainly shaped under the force of Enceladus' gravity, following approximately ballistic trajectories. Thus, the Cassini measurements of the grain size distribution at various altitudes directly constrain the grains' ejection speed distribution and the source mechanism.

The depletion of larger and/or heavier grains at higher altitudes observed in near-infrared spectra (Hedman et al., 2009) indicates that these grains are less likely to reach higher altitudes because of slower ejection speeds. This behavior is reproduced with a grain condensation model,

in which ice grains form at nozzles in the subsurface vents when the vapor pressure reaches saturation, and are then transported upward by the gas flow as they grow through accretion (Schmidt et al., 2008). However, the grains' ascent is hampered by wall collisions. After a collision, larger grains are accelerated more slowly back to the gas speed, because their surface-to-mass ratio is lower. The resulting effect is a size-dependent grain speed distribution when exiting the vents. Thus, the maximum height that a grain could reach depends on its size, which results in an altitude-dependent grain size distribution.

Plume stratification is also observed in the grain composition profile. The fraction of salt-rich ice grains (Type III) sharply increases from a few percent in the E ring to 40% near Enceladus' surface. This suggests that these grains, which are unable to escape into the E ring, are larger, likely flash-frozen water droplets (Postberg et al., 2009, 2011).

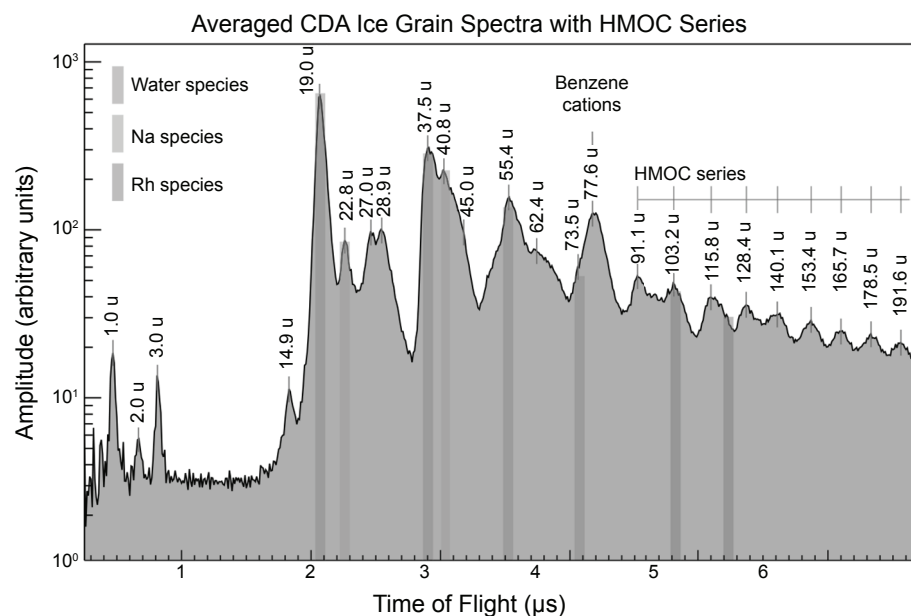


**Fig. 3.** Averaged mass spectrum of Enceladus ice grains with signatures of organic molecules seen by the Cassini CDA instrument (Postberg et al., 2018). In addition to cations associated with the benzene ring at 77 and 79 u, a series of so-called high mass organic cations (HMOC) cover a mass range from 91 to 200 u, and likely continue further outside the instrument mass range, indicating the presence of large organic molecules in Enceladus' subsurface ocean. Na species are due to salt in the grains; Rh species are due to the rhodium metal target of the CDA instrument.

Spacecraft Altitude  
and Ground Track  
*Hedman et al. 2018*

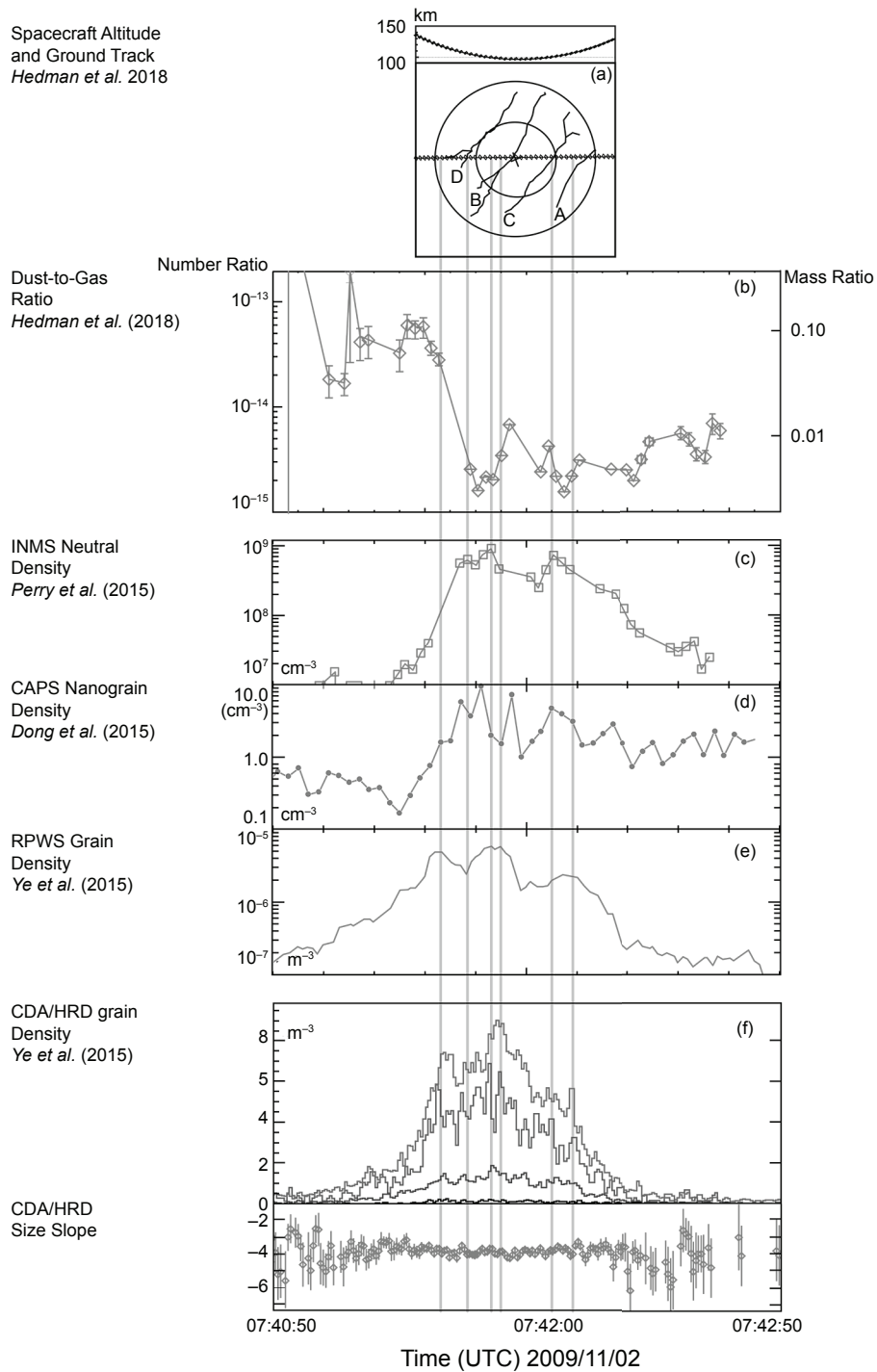


**Fig. 4.** Plume structure shown by the combined *in situ* gas and grain measurements during the Cassini E7 flyby on November 2, 2009. **(a)** Spacecraft altitude and ground track across the south polar terrain. Letters in gray are the first letter of each named tiger stripe, encountered in the flyby from left to right: Damascus (D), Baghdad (B), Cairo (C), and Alexandria (A). **(b)** The dust-to-gas number ratio and mass ratio as a function of time based on measurements shown in **(c)** and **(e)**. **(c)** Water vapor number density measured by the Cassini INMS instrument. **(d)** Negatively charged nanograin number density measured by the Cassini Plasma Spectrometer instrument. **(e)** Number density of micrometer-sized ice grains measured by the Cassini RPWS instrument. **(f)** Number density and size slope of micrometer-sized ice grains measured by the Cassini CDA instrument. The four different curves represent the number densities of grains with radii larger than 1.7, 2.2, 3.0, and 6.5  $\mu\text{m}$ , respectively. The grain size distribution is consistent with a power-law distribution with a slope of  $-4$ . Vertical lines mark the time when the density peaks in either water vapor or micrometer-sized grain profiles. These figures are modified from *Ye et al. (2014)*, *Dong et al. (2015)*, *Perry et al. (2015)*, and *Hedman et al. (2018)*.

Stellar and solar occultation measurements (Hansen et al., 2006, 2008, 2011, 2017) indicate that there are multiple narrow, supersonic gas jets embedded within a broad plume gas emission. The jet speed is roughly  $1.5\times$  the water vapor thermal speed ( $\sim 500\text{ m s}^{-1}$  at 273 K) (Tian et al., 2007; Hansen et al., 2008; Hurley et al., 2015), and the jet locations are spatially correlated with the grain density profiles as shown in Fig. 4 (Hansen et al., 2011; Ye et al., 2014; Dong et al., 2015; Perry et al., 2015; Hedman et al., 2018). Two models, based on Cassini images, have been proposed to describe the emission of a mixture of water vapor and ice grains: the “jet model” of  $>100$  discrete jets (Porco et al., 2014), and a “curtain model” where broad, curtain-like eruptions may explain both the apparent jets and broad emission (Spitale et al., 2015). The true plume environment at Enceladus may indeed be a combination of both. The dust emission through fast jets contributes significantly to replenishing the E ring (Mitchell et al., 2015), while the low-speed gas emission, stemming from sublimation (Goguen et al., 2013) or a layer at thermal equilibrium in contact with the fissure walls, also has a nonnegligible contribution (Perry et al., 2015; Teolis et al., 2017).

During the Cassini era, Enceladus’ total mass output rate was estimated to be about  $200\text{ kg s}^{-1}$ , ranging from  $100$  to  $1000\text{ kg s}^{-1}$  (Tian et al., 2007; Burger et al., 2007; Smith et al., 2010; Hansen et al., 2011; Dong et al., 2015; Teolis et al., 2017). Most of the output mass is gas, with micrometer-sized grains comprising only tens of kilograms per second (Gao et al., 2016; Southworth et al., 2017, 2019; Porco et al., 2017). Because of the previously described dynamical stratification, the local dust-to-gas mass density ratio could be closer to unity at altitudes below 25 km, such that grains may influence the dynamics of the ascending gas (Hedman et al., 2018). The mass flux and dust-to-gas ratio also vary at different tiger stripes (Fig. 4) (Kempf et al., 2008; Jones et al., 2009; Ye et al., 2014; Dong et al., 2015; Dhingra et al., 2017; Hedman et al., 2018), implying different properties in their sources or in the connections to the subsurface reservoirs.

## 2.4. Variability

The plume varies with Enceladus’ orbital phase. It is brightest near orbital apocenter (the furthest point from Saturn in Enceladus’ elliptical orbit) by a factor of  $\sim 5$  (Hedman et al., 2013). This implies that tidal stresses regulate its emission (in addition to supplying energy required for Enceladus’ activity; see section 4). Along Enceladus’ slightly eccentric orbit, the level of crustal stress from deformation due to tides raised by Saturn varies. This is thought to modulate the width of fissures, and thus the ejection of grains (Hedman et al., 2013; Nimmo et al., 2014; Perry et al., 2015; Porco et al., 2018). Ultraviolet occultation measurements suggest a larger water emission in the jets when Enceladus is near its orbital apocenter. However, such enhancement does not result in a substantially higher plume water vapor density (Hansen et al., 2017). The tidal control of plume activity

seems to be limited at the jets, modulating the emission of gas and dust across Enceladus’ orbital phase (Hedman et al., 2013; Nimmo et al., 2014; Hansen et al., 2017).

Temporal variabilities other than the diurnal modulation were also observed, from jets appearing in only a few minutes (Spitale et al., 2017) to a factor of 4 decrease of the plume brightness (dust content) from 2005 to 2015 followed by a subsequent increase (Ingersoll and Ewald, 2017; Porco et al., 2017). The mechanisms causing the plume’s long-term variability remain unclear, but could be tied to orbital resonances with Dione (Porco et al., 2017).

The plume must have been active since the detection of the OH torus around Saturn (Shemansky et al., 1993; Jurac et al., 2001) and the discovery of the E ring (Feibelman, 1967), and likely much earlier based on E-ring grain dynamics (at least a few hundred years) (Horanyi et al., 2008) and the level of crater degradation (Kirchoff and Schenk, 2009; Kempf et al., 2010). The central tiger stripe could be at least 0.1 to 1 m.y. old, based on a model in which the additional parallel stripes form because erupted ice grains that fall back onto the surface pile up along the sides of the central stripe, breaking long pieces of ice shell under their weight (Hemingway et al., 2020). On geological timescales, Enceladus’ activity may be episodic, as indicated by surface features and geophysical modeling (O’Neill and Nimmo, 2010; Spencer and Nimmo, 2013; Crow-Willard and Pappalardo, 2015). Considering heating from tidal dissipation in Enceladus’ porous rocky core, a geophysical model suggests that the observed activity could be supported for tens of millions to billions of years (Choblet et al., 2017). Over 1 b.y., a  $200\text{-kg s}^{-1}$  plume would eject about 5% of the mass of Enceladus, with 10% of this mass falling back to the surface (Schmidt et al., 2008).

## 3. TRACING THE PLUME TO THE OCEAN BELOW

### 3.1. Long, Narrow Channels with an Underground Source

As discussed in section 2, the plume composition and structure strongly indicate a subsurface ocean source. This is also supported by physical measurements and modeling. Cassini observations reveal that the tiger stripes are emitting gas at both high (up to Mach 10 or  $6\text{ km s}^{-1}$ ) and low ( $<1\text{ km s}^{-1}$ ) speeds (Teolis et al., 2017). The high-Mach gas is probably accelerated by the pressure gradient along the fissure length or through nozzle-like throats within the fissure. The low-Mach gas is either not accelerated in the fissures or has achieved thermal equilibrium by friction or thermal exchange with the fissure walls. Modeling indicates that high-Mach gas is best achieved by narrow jets with high aspect ratios (Yeoh et al., 2017). Narrow spreading angles argue against sublimation from ice on the surface of Enceladus as the source of the plume, and instead suggest a deep underground source where the vapor has to move



through long, narrow cracks before escaping. A turbulent dissipation model also suggests that the ocean-surface connection may be sustained on million-year timescales (*Kite and Rubin, 2016*).

Other aspects of the ocean-plume connection are much less constrained. Equilibrium thermodynamic and fluid mechanical modeling suggests that the vents are drawing from a deep subsurface liquid reservoir through a conduit, similar to explosive volcanic eruptions on Earth (*Mitchell et al., 2014*). The throat of the vent is likely to be the point of peak pressure (*Mitchell et al., 2017*). As ocean water and volatiles ascend through the conduit, the drop in temperature and pressure leads to boiling and freezing. These can occur together below the triple point pressure in the ocean water, according to the ratio of latent heat of evaporation to latent heat of fusion (*Mitchell et al., 2014*). Modeling suggests that this can lead to a solid:vapor ratio similar to that observed in the plume jets [ $\sim 6:1$ ; note that only  $\sim 4\%$  of the estimated  $200 \text{ kg s}^{-1}$  mass flux comes from the jets (*Porco et al., 2014*)], but this model neglects exsolution (dissolved gases returning to the gas phase) by volatiles other than  $\text{CO}_2$  and heat exchange during expansion. During ascent, gas and grains could also exchange momentum with each other and with the channel walls via sticking and nonsticking collisions. Salt grains could act as condensation nuclei and grow in size. Some particles may shrink in size as volatiles ( $\text{CO}_2$ ,  $\text{CH}_4$ , etc.) sublimate. Triboelectric charging (accumulation of positive or negative charge due to contact, separation, or friction) could occur for small (nanograin) particles (section 2.2), possibly leading to chemical reactions (called tribochemistry) on their surfaces. Such processes should be taken into account when analyzing plume composition and inferring properties of the ocean. Further modeling efforts (including exsolution and sublimation effects of many volatile species, etc.) and experimental work would improve the understanding of the connection between the ocean and the vents.

Organic enrichment processes may be occurring at the interface between the ocean and the icy crust of Enceladus. The  $\sim 3\%$  of E-ring grains bearing complex organic molecules (*Postberg et al., 2018*) (see section 2) have a high abundance of these organics (about 1% by mass) but a very low abundance of salts, suggesting that the organic molecules are hydrophobic and/or sourced from a salt-poor matrix. In Earth's polar regions, clouds of ice particles enriched in organic material and depleted in salts are generated by sea-spray aerosols (also termed "atmospheric marine aerosol"). Wave breaking leads to the bursting of air bubbles at a sea-surface microlayer of organic material floating on the ocean surface (*Burrows et al., 2014*). The submicrometer sea-spray aerosol thus generated is enriched 10 to 1000-fold in organic material. A similar process could occur on Enceladus, where aerosols formed at the water-ice interface due to rapid boiling beneath the jets could emerge from a boundary layer of organic material (*Postberg et al., 2018; Porco et al., 2017*). Such a process could also concentrate hy-

drophobic biosignatures such as lipids and fatty acids, if present (*Cable et al., 2017*).

### 3.2. What the Plume Tells Us About the Ocean

Measurements of the plume can be combined with Cassini gravity measurements and models of Enceladus' internal structure to provide constraints on ocean composition, pH, and temperature. For ocean temperature, the presence of salts such as NaCl — at concentrations constrained by CDA measurements of the flash-frozen, salt-rich grains in the plume (*Postberg et al., 2009*) — leads to freezing point depression, such that the minimum temperature is likely in the range of  $-1^\circ\text{C}$  (*Glein et al., 2018*). While other "antifreeze" agents such as  $\text{NH}_3$  are present, they are not likely present in the ocean at sufficient concentrations to depress the temperature further (*Porco et al., 2006; Glein et al., 2018*).

The pH of the Enceladus ocean has been constrained to  $\sim 9$ – $11$  (Fig. 5), using a thermodynamic model of carbonate speciation based on three sets of measurements: (1) sodium chloride and carbonate abundances in plume particles measured by CDA, (2) the existence of silica nanograins (*Hsu et al., 2015; Sekine et al., 2015*), and (3) the amount of  $\text{CO}_2$  in the plume gas measured by INMS (*Glein et al., 2015, 2018*). The simplest model geochemical system consistent with these measurements is a Na-Cl- $\text{HCO}_3/\text{CO}_3$  solution with alkaline pH. The pH range of this observation-based study is consistent with the first-principles approach of *Zolotov (2007)*, who assumed that Enceladus' ocean composition results from the aqueous alteration of carbonaceous chondrite material, a plausible analog of Enceladus' initial "rock" (nonvolatile) component (section 4.3). Notably, the pH of aqueous systems is temperature-dependent in a chemically closed system, so the hydrothermal fluid pH might be lower than the ocean, possibly in the range of 8–9 (*Sekine et al., 2015*). However, this might not be the case if the ocean is chemically open to the icy crust through effective volatile exchange; in that instance, the hydrothermal fluids might have a pH close to or higher than the ocean. Similar geochemical modeling efforts with more quartz-rich compositions (quartz-magnesite-talc) constrain the pH to  $<10$  and would be consistent with the observed silica nanograin abundance, while supporting a lower temperature ( $165^\circ\text{C}$ ) in the source region of the nanoparticles (*Glein et al., 2018*).

Currently, efforts to fully describe the hydrothermal geochemistry of Enceladus are confounded by the discrepancy between the  $\text{H}_2$  detection in the plume (meaning reaction with reduced minerals deep in the core, such as iron-bearing silicates) and the presence of silica nanograins (possibly sourced from quartz-rich rocks at shallower depths). No single water-rock interaction can produce both species:  $\text{H}_2$  and  $\text{SiO}_2$ . *Glein et al. (2018)* propose a scenario where hydrothermal fluids react at depth with iron-bearing rocks, picking up dissolved  $\text{H}_2$ , and then flow up through quartz-rich carbonates to obtain dissolved silica



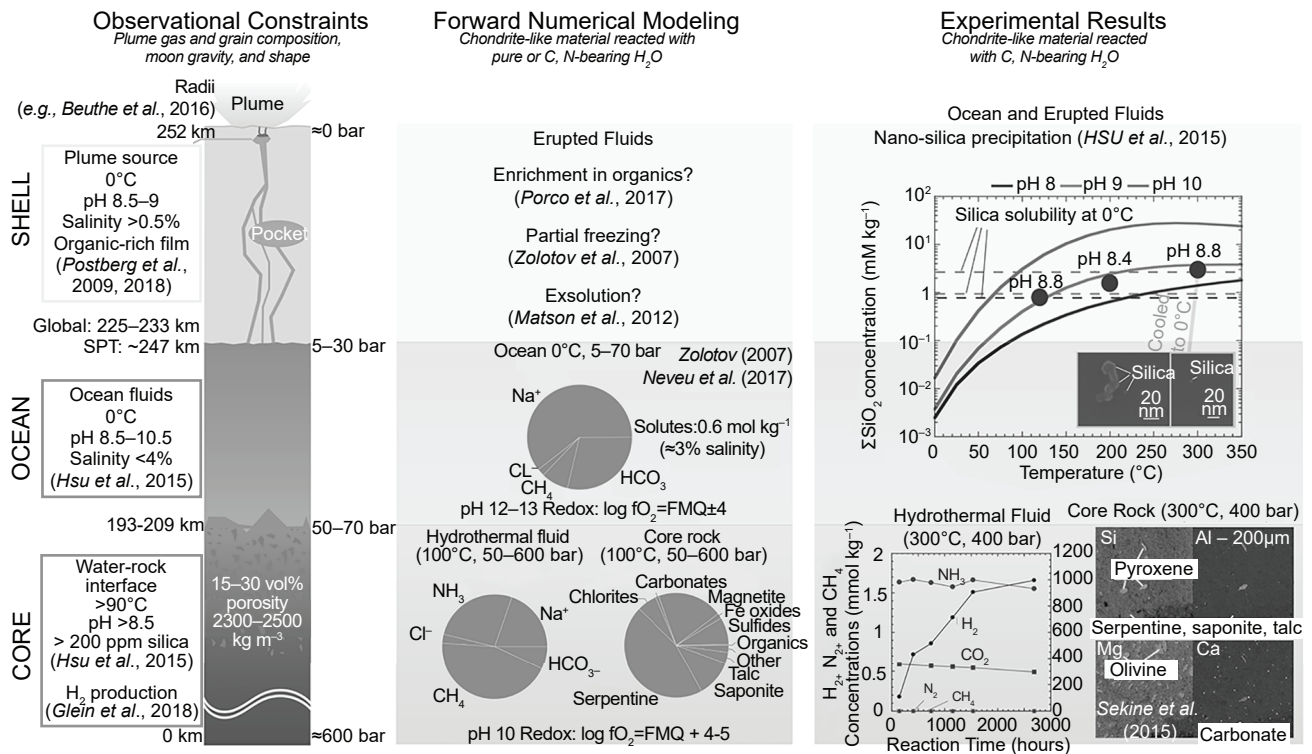


**Fig. 5.** See Plate 20 for color version. Physical and chemical connections between the plume, the ocean, and the core as evidenced by converging observational (section 3), modeling (section 4), and experimental results. SPT = south polar terrain.

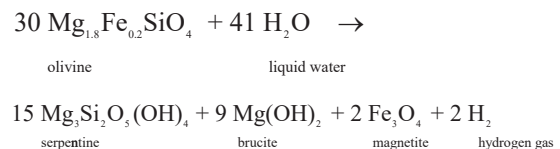
before flowing into the ocean and eventually expressing both species in the plume. Further experimental work is needed, as well as *in situ* measurements at Enceladus, to fully understand the complex geochemistry of this moon.

The high pH of Enceladus' ocean has several implications. First, serpentinization (reaction of water with ultra-mafic rocks such as olivine and pyroxene, often resulting in the generation of  $H_2$ ), which results in alkaline fluids, has most likely occurred or is still occurring on Enceladus (section 4). This is supported by the reported detection of  $H_2$  in Enceladus' plume by INMS (Waite et al., 2017). Second, alkaline conditions indicate that hydroxide ( $OH^-$ ) should be fairly abundant, and (bi)carbonate ( $HCO_3^-/CO_3^{2-}$ ) or sodium (bi)carbonate ( $NaHCO_3/Na_2CO_3$ ) should be the dominant forms of dissolved inorganic carbon. Third, divalent metals ( $Ca^{2+}$ ,  $Mg^{2+}$ ) should be present only at low concentrations (insoluble). Finally, organic acids, if present, will be deprotonated (negatively charged) and should be frozen inside plume particles as sodium or potassium salts, and ocean-derived amines will be neutral and may be detectable in the plume gas if sufficiently volatile. These last two points might drive mission design or the selection of a future instrument suite to Enceladus (section 6).

#### 4. CORE-OCEAN INTERACTION AND EVOLUTION

The potential for Enceladus to harbor life not just today, but also at any time since its accretion, is most likely controlled by the nature and extent of the interaction between

liquid water and rock. By “rock,” we refer to the nonice solids, which likely comprise mainly silicates, refractory organics, and metals including their sulfides and oxides. Water-rock interfaces provide, at least initially, locales of chemical disequilibrium between relatively oxidized (electron-poor) fluid and relatively reduced (electron-rich) rock. Reactions lead to reduction of fluid volatiles and oxidation of rock minerals and organics. In particular,  $H_2$  results from the reduction of  $H_2O$  concomitant with the oxidation of Fe species (Abrajano et al., 1990; Sherwood Lollar et al., 1993; Sleep et al., 2004). An example of a relevant reaction is (McCollom and Bach, 2009)



The synthesis of organic compounds of intermediate oxidation states from (bi)carbonate (McCollom and Seewald, 2007; McDermott et al., 2015), can be achieved by reactions such as (here, for carbohydrates)



The complete reduction to methane ( $HCO_3^- + 4 \text{ H}_2 \rightarrow \text{CH}_4 + \text{OH}^- + 2 \text{ H}_2\text{O}$ ) proceeds slowly (Sherwood Lollar et al., 2002) unless bio-mediated (Taubner et al., 2018) or catalyzed, typically by metals (McCollom, 2016). Thus, core-ocean interaction likely governs the supply of chemical

energy and key bioavailable elements, i.e., the habitability of Enceladus. To constrain Enceladus' astrobiological potential, it is therefore essential to understand to what extent the core and ocean interact, how long such interaction has taken place, and what chemical reactions can be predicted or inferred to be taking place.

#### 4.1. Present-Day Setting and Extent of Water-Rock Interaction

Measurements of Enceladus' gravity (*Jess et al.*, 2014), shape, and libration (*Thomas et al.*, 2016) suggest that its interior comprises a rocky core surrounded by a global ocean thicker at the south pole, underlying an ice shell. The global ice shell thickness is estimated at 20 to 25 km (*Beuthe et al.*, 2016; *Čadek et al.*, 2016), but it is much thinner (2–15 km) at the south pole (*Čadek et al.*, 2019; *Patthoff et al.*, 2019; *Hemingway and Mittal*, 2019). The core density, estimated at 2300 to 2500 kg m<sup>-3</sup> (*McKinnon*, 2015; *Čadek et al.*, 2016), is low compared to the densities of silicate grains: 2900–3000 kg m<sup>-3</sup> for hydrated, serpentine-rich silicates, with some variation depending on the Fe/Mg ratio (*Tyburczy et al.*, 1991; *Auzende et al.*, 2006) and higher for dry silicates (*Chung*, 1971; *Yomogida and Matsui*, 1983; *Consolmagno and Britt*, 1998). Thus, even if the rock is hydrated silicate, the core also comprises material of lower density, such as 15–30 vol% of water, or >30 vol% of refractory organics with density 1500–1700 kg m<sup>-3</sup> (*McKinnon et al.*, 2008; *Castillo-Rogez et al.*, 2012). The presence of water in the core is compatible with water-rock interaction as suggested by the chemistry of vented material (*Hsu et al.*, 2015; *Sekine et al.*, 2015; *Waite et al.*, 2017; *Glein et al.*, 2018). Similar core densities are expected for other icy worlds with a shape close to hydrostatic equilibrium (where gravity is balanced by internal pressure) and a radius below 800 km (Table 3), suggesting that waterlogged rocky cores may be the norm for such worlds.

The likely significant water content of Enceladus' core suggests that water-rock interaction is not restricted to the seafloor, but may instead be pervasive throughout the core. This is consistent with the expected low strength of the core because of low central pressures (<500 bar or 50 MPa) on this small, low-gravity world (*Neveu et al.*, 2014; *Klimczak et al.*, 2019). Two classes of models have been suggested for the water-rock interface: a core of cemented rock, but with porosity that either remains from accretion at low gravity or arises from fracturing processes (*Vance et al.*, 2007; *Neveu et al.*, 2014, 2015), or a core in which rock grains can move relative to one another with the water fluid (*Roberts*, 2015; *Choblet et al.*, 2017; *Bland and Travis*, 2017). The models are not mutually exclusive, as the rock fraction could increase with depth into the core to yield cemented, porous central regions surrounded by unconsolidated rock.

Regardless of the exact structure, a waterlogged core helps maintain the ocean because it is amenable to convective fluid circulation that both enhances tidal dissipation (*Choblet et al.*, 2017) and more efficiently transfers heat

out of the core compared to conduction alone (*Neveu and Rhoden*, 2019). As a result, core temperatures may be rather homogeneous with spatial variations not exceeding 100 K (*Choblet et al.*, 2017; *Neveu and Rhoden*, 2019). Still, ≥90 K gradients must exist between the freezing interface at the bottom of the ice shell (−1°C) and the deep sites able to solubilize the aqueous silica detected as nanograins (>90°C) thought to have precipitated when mixing with colder water (*Hsu et al.*, 2015; *Sekine et al.*, 2015) (Fig. 5 and section 2.2). To sustain such gradients, Enceladus' core must not be too permeable, as higher permeabilities favor more vigorous fluid flows that tend to homogenize temperatures (*Phillips*, 1991; *Neveu et al.*, 2015).

#### 4.2. Core-Ocean Interaction Through Time

The age of Enceladus' ocean is key to its ability to sustain life: too young, and there may not be enough time for life to emerge; too old, and chemical disequilibria (life's energy source) may have dissipated. The odds of us seeing Enceladus during a brief episode of unusually high activity are very low. Yet, how can this tiny world sustain such activity given its limited sources of endogenic (chiefly radioactivity) and exogenic energy (chiefly tidal dissipation) at the present day (*Meyer and Wisdom*, 2007), let alone through geologic time?

**4.2.1. The origin of Enceladus.** An upper bound on the age of Enceladus' ocean is the age of Enceladus itself. In the past few years, multiple new scenarios for the origin and evolution of Enceladus and Saturn's other mid-sized moons have been proposed. The result of these many plausible theories is that the spectrum of possible evolution scenarios for Enceladus and the other mid-sized moons of Saturn is vast (Fig. 6). Enceladus' ocean may have been interacting with the rocky core since the dawn of the solar system, or we may be witnessing a fluke lasting only decades to centuries.

In the canonical scenario, the moons formed in Saturn's subnebula at the dawn of the solar system 4.5 b.y. ago (*Mosqueira and Estrada*, 2003a,b). However, this might yield several larger (Titan-sized) moons, more akin to the Jupiter system than to what is seen at Saturn (*Canup and Ward*, 2006; *Crida and Charnoz*, 2012). Instead, Enceladus and its sibling moons could have formed from the debris of a Titan twin, disrupted after migrating too close to Saturn and dragged in by the remaining subnebular gas (*Canup*, 2010). Such a large moon would have already undergone ice-rock differentiation, and its core could have fallen into Saturn (*Canup*, 2010), leaving behind icier material to assemble the mid-sized moons we see today. If some metal-rock differentiation happened, metal-poor rock would be left over. Although this scenario reproduces the inner Saturn system, forming moons that are sufficiently rock-rich would require random delivery of rock by external impactors such as large comets (*Salmon and Canup*, 2017), which would provide further chemical mixing.

In yet a later formation scenario, Enceladus and its neighbors formed as ring material spread out (*Charnoz et al.*,

TABLE 3. Core densities of icy worlds estimated from spacecraft measurements or telescope observations.

Object	Mean Radius (km)	Core Density (kg m <sup>-3</sup> )	Reference
Enceladus*	252	2300–2500	<i>Hemingway and Mittal (2019)</i>
Ceres	470	2426–2439	<i>Ermakov et al. (2017)</i>
Dione	561	2300–2575	<i>Beuthe et al. (2016)</i>
Rhea	763	1240–2350†	<i>Tortora et al. (2016)</i>
Haumea	798	2550–2750	<i>Dunham et al. (2019)</i>
Europa	1561	Unconstrained (2500–3900 near seafloor)	<i>Schubert et al. (2009)</i>
Titan	2576	Unconstrained (2500–4500)	<i>Coyette et al. (2018)</i>

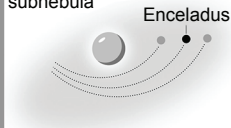
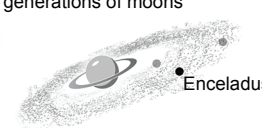
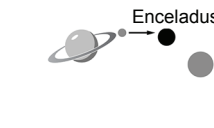
\* Because no gravity measurements have been made for Enceladus' neighboring moons Mimas and Tethys, the size of Mimas' core is unconstrained and Tethys' internal structure is unknown.

† Inferred from the reported range of possible core sizes (*Tortora et al., 2016*).

2011). This assumes that Saturn's rings predate the moons, which is debated (*Iess et al., 2019; Crida et al., 2019*), but in any case there may have been previous rings from disrupted moons. In this scenario, the moons form layered with a rock-rich core accreted first, being more resistant than ice to tidal disruption close to Saturn. Moreover, the closer-in

moons (Mimas, Enceladus) are younger than their outer siblings (Rhea), possibly by billions of years.

A final scenario suggests Enceladus is staggeringly young, perhaps only a few tens to hundreds of millions of years old (*Cuk et al., 2016*). This estimate is based on the absence of dynamical signatures of past moon-moon orbital

Formation Scenario	Primordial in Saturn subnebula 	From debris of previous generations of moons 	Late, from current rings 
Initial Composition	Homogeneous mixture of chondritic rock and cometary ice	Homogeneous rock and ice mixed from previous generation of moons	Cometary dust/ring pollution Ring ice
Age of the Ocean	?	?	Young
Problems	Architecture of moon system (produces jovian-like system)		Rings may be younger than time required for Enceladus to migrate out of its current orbit
Outstanding Questions	<ul style="list-style-type: none"> <li>•When did differentiation occur?</li> <li>•How much water-rock interaction/chemical equilibrium dissipated during differentiation?</li> </ul>	<ul style="list-style-type: none"> <li>•What was the starting chemistry of rock and ice?</li> <li>•When did differentiation occur?</li> <li>•How much water-rock interaction/chemical equilibrium dissipated during differentiation?</li> </ul>	Is equilibrium tidal heating sufficient to explain current ocean?

**Fig. 6.** Possible scenarios for Enceladus' origin and evolution. These control the timing, extent, and starting material composition of water-rock interaction, and therefore the extent of the habitability of Enceladus. These scenarios are not mutually exclusive and may have happened in sequence through time, from left to right, in which case Enceladus would be the product of the latest formation scenario.

resonances, indicating the moons formed later than when the resonances should have occurred, placing upper bounds on the ages of moons such as Enceladus.

**4.2.2. Sustaining the ocean.** Keeping water liquid inside Enceladus requires heat. Enceladus' main heat source likely arises from the dissipation of tides raised by Saturn (e.g., *Spencer and Nimmo*, 2013). Explanations for observed high levels of dissipation have been sought both in the way Enceladus' interior material responds to tides (*Tyler*, 2014; *Roberts*, 2015; *Choblet et al.*, 2017) and in variations of the orbital tidal forcing (*Travis and Schubert*, 2015; *Cuk et al.*, 2016). The main challenge in modeling Enceladus' internal evolution through time is that tidal dissipation couples geophysical and orbital processes, which act on vastly different timescales. Enceladus orbits Saturn with a period of just 32.9 hours (1.37 Earth days), and accurately simulating gravitational perturbations to its orbit from Saturn, the rings, and other moons requires computing interactions between each of these bodies and Enceladus hundreds of times per orbit (*Zhang and Nimmo*, 2009). This is not practical to simulate over the >4.5 b.y. of solar system history. Thus, in detailed dynamical simulations, the interior structure is usually simplified to a point mass with tidal dissipation and deformation averaged over the entire moon (e.g., *Meyer and Wisdom*, 2007; *Cuk et al.*, 2016). In detailed geophysical simulations, orbital properties are at least simplified (*Neveu and Rhoden*, 2019) and usually fixed (*Choblet et al.*, 2017), varied arbitrarily (*Travis and Schubert*, 2015), or ignored (*Schubert et al.*, 2007).

Another challenge is that essential quantities for Enceladus remain largely unknown. A dynamical example is the internal structure and propensity for tidal dissipation of Saturn, which determines how Enceladus' orbit and tidal forcing change over time (*Fuller et al.*, 2016; *Lainey et al.*, 2017; *Nimmo et al.*, 2018). A geophysical example is the estimation of mechanical properties of ice (*McCarthy and Cooper*, 2016; *Renaud and Henning*, 2018) and rock-ice mixtures (*Choblet et al.*, 2017) at relevant temperatures, stresses, and strain rates based on experiments (*Durham et al.*, 1992, 2010), necessarily limited in parameter space and timescale.

**4.2.3. Observational clues.** Perhaps a meaningful upper bound on the ocean age can be inferred from the fact that chemical reactions seem to still be happening (*Hsu et al.*, 2015; *Waite et al.*, 2017); chemical equilibrium has yet to be achieved. At the temperatures of 50° to 100°C required to keep silica soluble in order to then precipitate silica nanograins in colder fluids (*Hsu et al.*, 2015; *Sekine et al.*, 2015), chemical reactions should proceed very quickly relative to the age of the solar system. On Earth, water-rock reactions that complete the abiotic reduction of carbon all the way to methane seem to proceed on ~1-b.y. timescales below 100°C (*Etioppe and Sherwood Lollar*, 2013). In this case, the path to equilibrium may be limited by how fast unreacted rock is exposed to ocean fluids. The distance traveled by a fluid front diffusing through rock increases with the square root of time (*McDonald and Fyfe*, 1985).

Equivalently, the timescale of alteration can be understood as the time taken by a fluid front to travel halfway between two adjacent water-rock interfaces (cracks or pores, or edges of rock chunks). Experiments suggest that the front travels about 1 m in about 10<sup>6</sup> yr, or 1 mm (the size of larger grains in chondrites) in a few years (*McDonald and Fyfe*, 1985). Thus, Enceladus' interior may not reach equilibrium readily if some of its core is cemented, shielding part of the rock from alteration. If adjacent fluid paths are no closer than ~20 m, some rock would remain unreacted over the age of the solar system. Comparatively, reactions do not seem limited by the availability of unreacted fluid, unless circulation through the core is much slower than fluid transport of silica and H<sub>2</sub> tracers of water-rock reactions, which are transported through the ocean and shell and vented to space within months (*Hsu et al.*, 2015; *Waite et al.*, 2017).

No matter when the current ocean was emplaced, Enceladus seems to have had episodic strong internal heating [ $>150 \text{ mW m}^{-2}$  (*Bland et al.*, 2012)], akin to today's [ $\sim 400 \text{ mW m}^{-2}$  (*Howett et al.*, 2011)]. Evidence for episodic high heat flow is recorded in surface craters that are smoothed out (relaxed), yet relatively old because they are overprinted by younger craters and fractures (*Bland et al.*, 2012) (Fig. 7). The relative chronology is the following: (1) Enceladus' surface is impacted, leaving behind sharp craters; (2) Enceladus experiences high internal heating and the warm ice softens, smoothing the crater morphology; (3) the surface cools down enough to prevent the healing of subsequent craters and fractures; (4) steps 2 and 3 are repeated to the present day such that several sets of relaxed craters and fractures overlap. Unfortunately, it is not possible to tell how much time this sequence of events took. If Enceladus' craters were caused by debris in the Saturn system, they may have occurred only a few 10–100 m.y. ago, but if the impactors orbited the Sun (as those that generated craters on the terrestrial planets, the Moon, main-belt asteroids, and Pluto), the craters would be billions of years old, and so would Enceladus (*Kirchoff et al.*, 2018).

### 4.3. Chemistry of Water-Rock Interaction

Unlike the age of the ocean, the chemistry of water-rock interaction is relatively well constrained. Chemical reactions between liquid water and rock arise from chemical disequilibria at water-rock interfaces at the physical conditions (temperature, pressure, water-to-rock ratio) of the setting. Fundamental considerations (the rocky material, if analogous to meteoritic, cometary, or interplanetary dust matter, is much more reducing than water or fluids that would result from melting cometary ices), analogies with settings of water-rock interaction on Earth, and measurements of the Enceladus plume and stream particle compounds attributed to products of water-rock reactions (*Hsu et al.*, 2015; *Waite et al.*, 2017) all suggest that oxidizing (electron-poor) fluids are interacting with reduced (electron-rich) rock. The resulting oxidation-reduction (redox) disequilibrium could provide a long-term source of chemical energy that, on



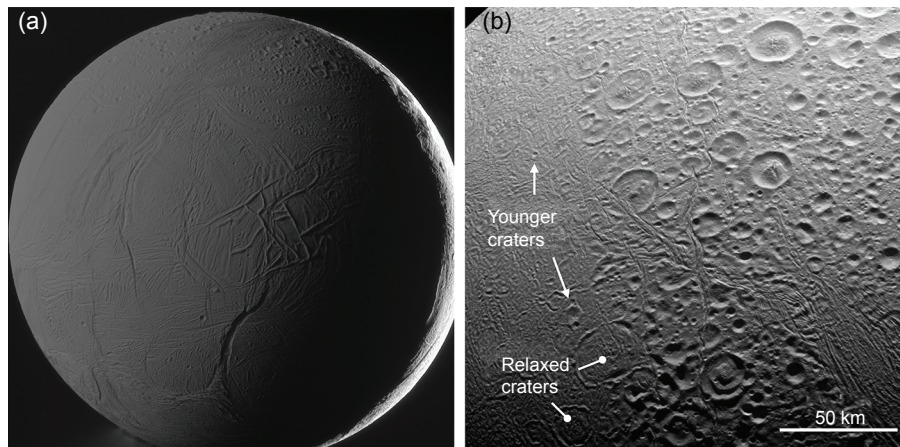


**Fig. 7.** (a) Enceladus' surface, illuminated by the Sun (crescent to the right) and sunlight reflected by Saturn, shows craters and fractures that overprint each other. Part of the south polar plume is visible at the bottom on the Saturn-lit side. (b) Zoom on a region near the north pole, showing how smooth craters overprinted by fractures and younger craters suggest past episodes of high heat flow (Bland et al., 2012). Credit: NASA/JPL-Caltech/Space Science Institute/G. Ugarković.

Earth, can sustain ecosystems deprived of sunlight (e.g., Schrenk et al., 2004).

The oxidized nature of Enceladus' fluids is suggested by the presence of  $\text{CO}_2$  in the plume (Waite et al., 2006, 2009, 2017) and the compositions of cometary volatiles (Bockelee-Morvan et al., 2004; Mumma and Charnley, 2011), which presumably represent the species accreted by icy moons (Mousis and Alibert, 2006). Additionally, the near surfaces of all airless bodies are subjected to photon and particle radiation, which can split  $\text{H}_2\text{O}$  to form reduced  $\text{H}_2$  and oxidants such as  $\text{H}_2\text{O}_2$  and  $\text{O}_2$  (Parkinson et al., 2008).  $\text{H}_2$  escapes owing to its low molecular mass, leaving behind an oxidant-enriched shell. Although Enceladus' ice shell seems too thin to allow convective transport of near-surface oxidants to the ocean (Barr and McKinnon, 2007), and the shell would resist any convective motion driving subduction (Howell and Pappalardo, 2019), oxidants could be buried under accumulating plume fall-out, perhaps all the way down the few kilometers to the ocean (Čadek et al., 2019; Patthoff et al., 2019). Finally, oxidants can be produced by radiolysis of water via energetic particles resulting from the decay of potassium, thorium, and uranium radioisotopes in the core (Bouquet et al., 2017). Potassium is also soluble in the ocean, as evidenced by the detection of  $\text{K}^+$  in the plume (Postberg et al., 2009), and could lead to oxidants via radiolysis in the ocean itself.

Enceladus' rocky core is likely to be much more reduced. Although the composition of the rock accreted by icy moons is unknown, a first guess is to extrapolate from recovered infall of primitive extraterrestrial material on Earth such as chondritic and/or carbonaceous (micro)meteorites and interplanetary dust particles. Chondritic material seems to have formed somewhat concurrently with planetesimals and giant planets in the first few million years of solar system history (e.g., Desch et al., 2018, and references therein), and therefore might have been accreted by primordial icy moons, with several caveats. First, the composition of rock may

not have been homogeneous across the early solar system regions where chondritic parent bodies and giant planets formed, even though there could have been mixing due to planetary migration (e.g., Walsh et al., 2011) and entrainment by nebular gas (Johansen and Lambrechts, 2017). Second, the giant planet subnebulae may have segregated material, potentially resulting in a different composition from material in the surrounding heliocentric (Sun-orbiting) protoplanetary disk (Alibert et al., 2005). The proportions of subnebular and heliocentric material inside Enceladus are unknown because of the uncertainty on Enceladus' origin (section 4.2). Finally, the material recovered on Earth is likely biased not just by provenance region in the solar system, but also toward the materials able to survive ejection from the planetary body, Earth entry, and impact, and therefore against volatile-rich material (Rivkin et al., 2014). Rock compositions in the Saturn system have also been informed by *in situ* analyses of ring particles made during the Grand Finale phase of the Cassini mission. These suggest that organic-rich ring particles are much more abundant than expected from earlier remote sensing (Waite et al., 2018; Hsu et al., 2018).

Another handle on possible fluid and rock compositions comes from numerical simulations of the interaction between fluid and rock initially at disequilibrium. Simulations of chemical equilibrium provide the end-member compositions toward which the system is driven, a necessary first step to understanding the fluid-rock system. These calculations, which seek to minimize the Gibbs free energy (amount of energy that can do work at given temperature and pressure), leverage measurements and extrapolations of thermodynamic properties for hundreds of species (e.g., Johnson et al., 1992, and references therein), and their accuracy hinges on the comprehensiveness of these data (Oelkers et al., 2009). Although most major species are covered, data for hydrated minerals are more uncertain (Oelkers et al., 2009), especially for species that are rarer on Earth but potentially common on Enceladus such as ammonium-bearing clays that

could sequester Enceladus' nitrogen (Neveu *et al.*, 2017). Whether equilibrium is achieved depends on kinetics along the path of reaction, which in turn depend on factors such as temperature, the extent of disequilibrium, concentrations of species such as  $H^+$  (pH), mineral surface properties, or the action of catalysts (e.g., Pokrovsky and Schott, 1999; Palandri and Kharaka, 2004). Kinetic data are available for fewer species, and usually do not capture dependencies other than temperature. Consequently, forward modeling efforts of water-rock interactions inside Enceladus to date have involved equilibrium simulations and only qualitative discussion of how kinetic limitations might affect the results.

The equilibrium products of reactions between chondritic rock and water were determined numerically by Zolotov (2007) at Enceladus conditions inferred from plume analyses. In that study, the hydrogen fugacity (effective partial pressure), a measure of the redox state, was set to match the  $CO_2/CH_4$  molar ratio of about 2 measured in the plume (Table 1). The system was assumed open with respect to  $H_2$ , to simulate  $H_2$  removal by escape to space. This assumption, plausible given Enceladus' low gravity ( $0.11 \text{ m s}^{-2}$  at the surface, about 1% of Earth's), leads to oxidized equilibrium fluid and rock. Predicted predominant minerals were, in order of volumetric abundance, saponite clay (e.g.,  $Mg_{0.17}Fe_3Al_{0.35}Si_{3.65}O_{10}(OH)_2$ ), serpentine ( $Fe,Mg_3Si_2O_5(OH)_4$ ), iron oxides (goethite  $FeOOH$  or magnetite  $Fe_3O_4$ ), iron sulfides (pyrrhotite  $FeS$  and/or pyrite  $FeS_2$ ), chlorite clay ( $Fe,Mg_5Al_2Si_3O_{10}(OH)_8$ ), calcite  $CaCO_3$ , and nickel sulfide. Minor phosphates, chromite, and carbonates (Ca,Mg,Fe,Mn)  $CO_3$  also result from simulations. Dominant solutes were  $Na^+$ ,  $Cl^-$ , and (bi)carbonate, followed by  $K^+$  and  $HS^-$ , in agreement with the findings of Na- and K-bearing salt grains in the plume (Postberg *et al.*, 2011), and indicating that the system was not so oxidized as to yield sulfate. This solution composition was not sensitive to water-to-rock mass ratios between 0.3 and 10 at  $100^\circ\text{C}$ . The fluid pH was alkaline, decreasing with temperature from 11 to 8, in agreement with the independent estimates of Glein *et al.* (2015, 2018) described in section 3.

These rock and fluid compositions are qualitatively similar to those determined by other studies (Schulte and Shock, 2004; Neveu *et al.*, 2017). Unlike the models of Zolotov (2007), these studies did not prescribe the redox evolution from plume data, but somewhat equivalently started from a carbonaceous chondrite mineralogy thought to have resulted from partial aqueous alteration and  $H_2$  escape on the parent bodies of these meteorites (when starting from a less-altered mineralogy, much  $H_2$  is produced). The agreement among models, albeit based in part on the same thermodynamic data, and with experimental results (Sekine *et al.*, 2015) and the limited plume measurements available, provides some confidence in our current understanding of Enceladus' interior chemistry (Fig. 6).

Nonetheless, even without new data, several improvements could be made to models or experiments seeking to reproduce the chemistry of Enceladus. First, in many models, the trapping of gases in clathrate hydrates (water cages) was

ignored. However, conditions at Enceladus' seafloor are expected to be in the stability fields of several clathrates (e.g., Mousis *et al.*, 2015), which tend to be more stable at higher pressures and lower temperatures. Sequestration in clathrates would delay or prevent gas escape, affecting the types and amounts of species dissolved in the ocean waters and expressed in the plume.

Second, models and experiments could consider other possibilities for the starting ice (fluid) and rock compositions if Enceladus is not primordial. In the formation scenario of Canup (2010) described in section 4.2, Enceladus' rock would be less rich in iron (less mafic) and reducing, perhaps more akin to what is expected at the seafloor of Europa [which likely has experienced metal-rock differentiation (Zolotov and Kargel, 2009; Schubert *et al.*, 2009)]. If Saturn's inner moons formed from ring material (Canup, 2010; Charnoz *et al.*, 2011), *in situ* ring analyses indicate that more organic-rich compositions may be warranted (Waite *et al.*, 2018; Hsu *et al.*, 2018).

Finally, it is crucial to better model kinetic limitations in reaching equilibrium, because kinetics likely influence the fate of bioessential elements and their bioavailability. For example, reduction of fluid  $CO_2$  to ultimately yield methane ( $CH_4$ ) does not easily proceed to completion (McCollom and Seewald, 2001; Sherwood Lollar *et al.*, 2002; Holland *et al.*, 2013; McCollom, 2016), but rather stalls at metastable organic compounds of intermediate oxidation states (Shock and McKinnon, 1993, and references therein), promoting organic synthesis (McCollom and Seewald, 2007). If  $CH_4$  formation is inhibited, forward models produce organic-rich fluids. Dominant C solute compounds are ethanol ( $CH_3CH_2OH$ ) and acetate ( $CH_3COO^-$ ), with less-abundant  $CH_3COOH$ ,  $NaCH_3COO$ ,  $NH_4CH_3COO$ , etc. (Shock and McKinnon, 1993; Schulte and Shock, 2004; Neveu *et al.*, 2017). Aqueous (bi)carbonate, aqueous  $CO_2$ , methanol  $CH_3OH$ , and formate  $HCOO^-$  are slightly less abundant. There is much less  $H_2$  production, as the reducing power is captured in the organics. Detection of diverse soluble organic compounds in the plume (Khawaja *et al.*, 2019) may support these processes.

In contrast and as evidenced by the detection of  $NH_3$  and potentially  $H_2S$  in the plume (Waite *et al.*, 2009), N and S species may be less affected by kinetics (Neveu *et al.*, 2017). This may not seem intuitive. Indeed, reduction of  $N_2$  to  $NH_3$  involves breaking the strong N-N triple covalent bond, which is slow in the absence of catalysts (e.g., Rodriguez *et al.*, 2011; Anderson *et al.*, 2013). Sulfate can persist for months at high temperature in reducing conditions (Mottl and Holland, 1978; Seyfried and Mottl, 1982) and likely orders of magnitude longer in cold fluids (Ohmoto and Lasaga, 1982). However, much N and S may already be reduced initially, as evidenced by observations of  $NH_3$  and  $H_2S$  in cometary gases [Mumma and Charnley (2011), but see Rubin *et al.* (2015) for a detection of oxidized  $N_2$ ] and N-bearing organics and sulfide minerals in chondrites (McKinnon and Zolensky, 2003; Alexander *et al.*, 2017). Thus, the presence of aqueous  $NH_3$  and  $NH_4^+$  and sulfide minerals should not be impeded by kinetics. However, the

release of N and S from organics ( $\leq 20\%$  of the initial N and S pool in carbonaceous chondrites) could be inhibited (Oh et al., 1988; Maffei et al., 2012, 2013).

In summary, chemical disequilibria likely arose at the time of accretion. They could be replenished to a limited extent by burial of oxidants to the subsurface ocean and radiolysis (Bouquet et al., 2017). The dissipation of disequilibria is likely limited by physical processes able to expose unreacted reduced rock to oxidizing fluids, and by chemical kinetics for some reactions such as those involving carbon oxidation/reduction. The dissipation of disequilibria causes alkaline conditions and promotes the synthesis of organics, which could provide available building blocks for prebiotic or biological synthesis.

## 5. ASTROBIOLOGICAL IMPLICATIONS

Observational and modeling constraints on conditions within Enceladus' ocean, and the physical and chemical processes that govern them, help to inform our understanding of the life-hosting potential of Enceladus — not only habitability but, in the case of an inhabited world, *detectability*.

A complete picture of biological potential should consider how processes and conditions would affect not only extant cellular life, but also its origin and evolution. The latter are discussed only briefly; our limited understanding of the origin of life and its environmental context, even on Earth, prohibit a more detailed discussion.

### 5.1. Origin of Life on Enceladus

Two prominent theories have different implications for the potential emergence of life on Enceladus. One theory posits that a three-phase (ocean-atmosphere-mineral) system favors, or may be essential for, the origin of life — in part because wetting-drying cycles can serve to concentrate organics, promote membrane self-assembly, and drive the formation of amino acid and RNA polymers (Deamer and Georgiou, 2015; Deamer and Damer, 2017). If this theory is correct, the origin of life on worlds that lack an atmosphere-water and atmosphere-mineral interface (e.g., Enceladus and other ocean-bearing icy moons) would be either disfavored or disallowed, depending on the stringency of the three-phase requirement.

Conversely, the “alkaline vent hypothesis” posits that life can and did originate in two-phase (ocean-mineral) systems (Lane and Martin, 2012; Russell et al., 2014). In this scenario, alkaline,  $H_2$ -rich fluids produced by serpentinization yield conditions favorable for the origin of life as they emerge into an ocean that is more acidic; the resulting pH gradient provides an energy source (modern life utilizes intracellular pH gradients to store and release energy), along with reducing power and mineral catalysts capable of reducing  $CO_2$  to organics that might be used by life. If this theory is correct, life could emerge on ice-covered ocean worlds that host the appropriate style of hydrothermal venting. As described in section 2, the presence of silica nanoparticles in Enceladus

plume materials is interpreted as evidence of hydrothermal venting (Hsu et al., 2015), and alkaline and  $H_2$ -rich conditions in the ocean (Glein et al., 2015; Waite et al., 2017) would be consistent with alkaline venting specifically. An Earth example of an alkaline vent is the ultramafic “white smoker” hydrothermal system Lost City on the Mid-Atlantic Ridge (Kelley et al., 2005), which is metabolically diverse; microbial cycling of sulfur and methane are the dominant active biogeochemical processes (Brazelton et al., 2006).

Beyond data that are consistent with the presence of alkaline vents, it is challenging to bring observational data to bear on the potential for emergence of life on Enceladus. The alkaline conditions inferred for the present ocean (sections 3 and 4.3) could confound the ability to produce hydrolysable polymers such as those used by Earthly life for both catalysis (proteins) and information processing (RNA and DNA), particularly at the higher end of the suggested range of pH 9–11 (Glein et al., 2018). Some organisms on Earth can tolerate pH as high as 13 [i.e., alkalithermophilic sulfate-reducing bacteria in Lake Calumet (Slonczewski et al., 2009; Roadcap et al., 2006)], but do so by virtue of cellular membranes and energy-expending mechanisms that make it possible to maintain intracellular pH at close to neutral levels and almost always  $< 9$  (Slonczewski et al., 2009). In the absence of such mechanisms, exposure to alkaline pH would considerably diminish the stability of hydrolyzable polymers, or indeed the ability to form them in the first place. For example, free solution rates of RNA hydrolysis are about  $5600\times$  higher at pH 11 than at pH 7 (Li and Breaker, 1999). However, modern ocean conditions need not, and probably do not, represent the prevailing conditions over the lifetime of the ocean. A better understanding of the potential implications of alkaline pH for the origin of life will depend on the ability to constrain the possible history of ocean pH from its earliest stages.

### 5.2. Cellular Life on Enceladus

Relative to the requirements and limitations expressed by extant life on Earth (see the chapter by Hoehler et al. in this volume), our understanding of Enceladus from Cassini data portrays Enceladus as a habitable world. Earthly life requires liquid water, a source of light or chemical energy, a supply of the major biogenic elements (carbon, hydrogen, oxygen, nitrogen, phosphorus, and sulfur) and various metals, and physicochemical conditions that support a range of biological molecules, structures, and processes. Cassini data bear directly on the availability of liquid water, chemical energy, and C, H, N, and O, constrain salinity, and support inference of ocean pH. The moon hosts an extensive liquid water ocean. Sodium chloride and silica nanoparticles sourced in the plume materials are both indicative of significant interaction of the ocean with Enceladus' rocky mantle (section 4), which could serve to supply both energy and materials to the liquid water environment. The simultaneous presence of  $H_2$  and  $CO_2$  represents a chemical energy source that is utilized by microorganisms on Earth. Carbon is abundant in



both oxidized and reduced forms, and nitrogen is abundant in a form — ammonia — that is readily oxidized by biology on Earth. While the physicochemical environment remains to be fully characterized, constraints on pH (Glein *et al.*, 2015, 2018; Waite *et al.*, 2017), temperature, and salinity (Postberg *et al.*, 2011) place those values within the biologically tolerated range (Rothschild and Mancinelli, 2001).

These data, of course, represent a qualitative “snapshot” of habitability on Enceladus that is applicable to extant, Earth-like life at the present moment: At least some organisms known on Earth would likely survive in the conditions that apparently now prevail on Enceladus. But habitability is an evolving, emergent property of the physical and chemical processes at work. These processes govern not only conditions, but *fluxes* of materials and energy that ultimately determine how large, diverse, and productive any biosphere on Enceladus could be. Although a truly quantitative picture of Enceladus’ biological potential must await a more detailed understanding of the processes at work there, some quantitative constraints are suggested by observations and modeling work.

The size and productivity of any biosphere on Enceladus would likely not be limited by the availability of carbon, nitrogen, or sulfur. Average cell abundance in Earth’s oceans is on the order of  $10^6$  cells  $\text{cm}^{-3}$  (Whitman *et al.*, 1998). Given the observed C, N, S, and P composition of typical aquatic cells (Fagerbakke *et al.*, 1996), the aqueous concentration of those elements that is equivalent to  $10^6$  cells  $\text{cm}^{-3}$  can be calculated and compared to their observed or inferred abundance in the plume or ocean of Enceladus (Table 4).

Reported abundances of  $\text{CO}_2$  and  $\text{NH}_3$  in the plume based on Cassini INMS data (Waite *et al.*, 2017) exceed biological requirements by 5–6 orders of magnitude.  $\text{H}_2\text{S}$  was reported in the plume at abundances of 12–34 ppm [vol:vol  $\text{H}_2\text{O}$  (Waite *et al.*, 2009)], about 5 orders of magnitude higher than the biological requirement, but the  $\text{H}_2\text{S}$  detection is considered ambiguous (Magee and Waite, 2017) because a range of other environmentally plausible compounds have nominally the same mass at the mass resolution of the INMS.  $\text{H}_2\text{S}$  abundance in the ocean has also been predicted via equilibrium geochemistry modeling (Zolotov, 2007), with a range, dependent on the temperature at which water-rock interaction occurs, of approximately  $5 \times 10^{-5}$  to  $5 \times 10^{-9}$  on a mol per mol  $\text{H}_2\text{O}$  basis. The low end of the range, corresponding to water-rock reaction temperature close to 273 K, still exceeds the biological requirement by more than an order of magnitude.

Possible phosphorus limitation of a biosphere on Enceladus has been suggested (Lingham and Loeb, 2018). The issue is not one of overall P abundance. Given the P content typical of aquatic cells on Earth [0.46–1.4 fg P cell $^{-1}$  (Fagerbakke *et al.*, 1996)] and an Enceladus ocean volume of  $2.7 \times 10^{16}$  m $^3$  (Steel *et al.*, 2017), a global ocean biosphere averaging  $10^6$  cells  $\text{cm}^{-3}$  could be constructed from  $3.5 \times 10^{13}$  g P. Ordinary chondrites contain 0.8–2 g P kg $^{-1}$  (Mason, 1979). Adopting the low (most conservative) end of the range, and assuming a silicate core density of 2400 kg m $^{-3}$  (Jess *et al.*, 2014) and a core radius of 182 km (Čadek *et al.*, 2016), the needed P would be supplied by the upper 43 mm of the silicate core, whereas the observed

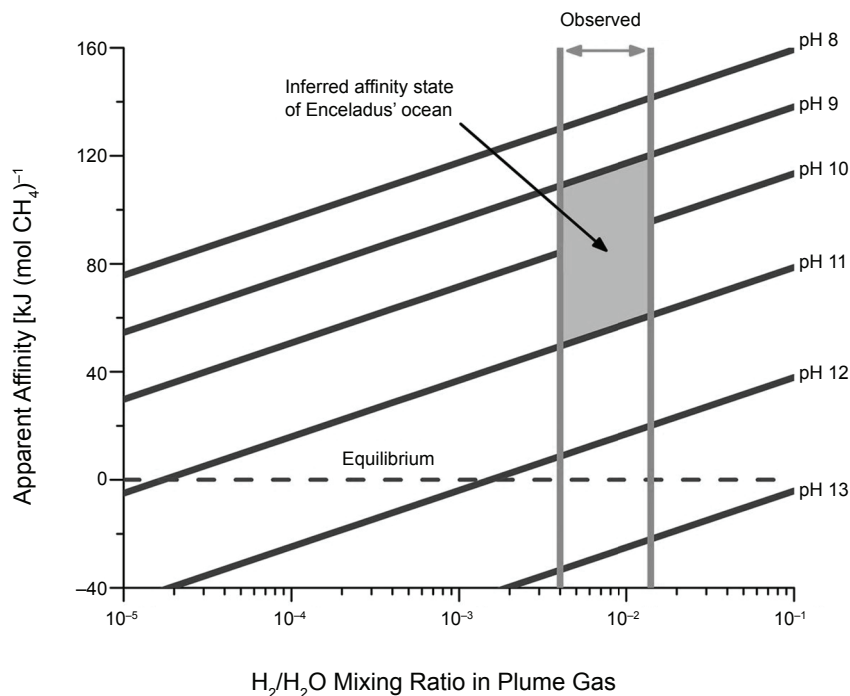


**Fig. 8.** Apparent affinity (Gibbs energy change) for methanogenesis in the ocean of Enceladus, constrained by ocean pH and the abundance of  $\text{H}_2$ . The shaded box lies above the dashed line for chemical equilibrium, meaning the ocean is in disequilibrium and therefore could support life. Reproduced from Waite *et al.* (2017).



TABLE 4. Comparison of elemental requirements for biology vs. abundances observed in the plume, or predicted via geochemical equilibrium modeling.

	C <sup>¶</sup>	N	P	S
Mass in a typical aquatic cell (fg)*	7–31	1.6–5	0.46–1.4	0.3–0.56
Required abundance for 10 <sup>6</sup> cells cm <sup>-3</sup> (mol per mol H <sub>2</sub> O) <sup>†</sup>	1.1–4.7 × 10 <sup>-8</sup>	2.1–6.5 × 10 <sup>-9</sup>	2.7–8.2 × 10 <sup>-10</sup>	1.7–3.2 × 10 <sup>-10</sup>
Plume observation (vol per vol H <sub>2</sub> O) <sup>‡</sup>	3–8.3 × 10 <sup>-3</sup>	4–13 × 10 <sup>-3</sup>	—	
Predicted ocean abundance (mol per mol H <sub>2</sub> O) <sup>§</sup>			<2 × 10 <sup>-12</sup>	5 × 10 <sup>-5</sup> to 5 × 10 <sup>-9</sup>

\* Fagerbakke et al. (1996).

<sup>†</sup> Seawater substrate concentration, expressed as moles of solute per mole of H<sub>2</sub>O, required to supply the elemental requirements of 10<sup>6</sup> cells cm<sup>-3</sup>.

<sup>‡</sup> Elemental abundance expressed as volume of species per volume of H<sub>2</sub>O, as calculated from mixing ratios of CO<sub>2</sub> and NH<sub>3</sub> (Waite et al., 2017) in the volatile component of the Enceladus plume. Volume:volume units are directly comparable to mol:mol units if plume volatiles behave as ideal gases. The calculation neglects the contribution of plume ice particles to total water efflux (estimated at ~4%) (Porco et al., 2017).

<sup>§</sup> Based on abundances plotted in Figs. 2 and 3 of Zolotov (2007).

<sup>¶</sup> As total inorganic carbon, the sum of CO<sub>2</sub>, HCO<sub>3</sub><sup>-</sup>, and CO<sub>3</sub><sup>2-</sup>.

NaCl content implies much more extensive dissolution of rock. However, P as phosphate — the form of P in the biomolecules of life on Earth — partitions dominantly into the silicate mineral phase, with calculations suggesting that equilibrium phosphate concentrations should be in the range of 10<sup>-11</sup>–10<sup>-10</sup> mol kg<sup>-1</sup> H<sub>2</sub>O (10<sup>-13</sup>–10<sup>-12</sup> mol mol<sup>-1</sup> H<sub>2</sub>O) at water-rock reaction temperatures of 150°–300°C, and lower still at lower temperatures (Zolotov, 2007). These concentrations would be insufficient to supply the P required for an average cell density of 10<sup>6</sup> cells cm<sup>-3</sup>, but could supply a 100-fold lower cell density. Importantly, low-equilibrium phosphate concentrations would not necessarily constitute a limit on biomass density, provided that ongoing water-rock processing can supply the ocean with a continuing, albeit small, flux of P that could be scavenged for the construction of biomass. However, it may stand as an important consideration for the origin of life, if the prebiotic synthesis of phosphate containing informational and energy-carrying molecules requires high concentrations of phosphate. This is an important area for progress in understanding the habitability of Enceladus.

In contrast to (non-P) bioessential element availability, energy availability may significantly constrain the possible size and productivity of a biosphere on Enceladus. Life on Earth is only known to utilize redox chemistry and near-infrared to visible light as sources of Gibbs (free) energy; other forms of energy are not known to be captured by life. Lacking direct access to solar radiation, any life within the Enceladus ocean would depend exclusively on whatever redox chemical energy the moon itself supplies.

Before considering how Enceladus may supply chemical energy for life, it is instructive to briefly review the two aspects of energy availability that impact life on Earth. First, chemical energy sources must represent a Gibbs energy change ( $\Delta G$ ) that makes their reaction not only chemically spontaneous ( $\Delta G < 0$ ) but also suitable for driving the end-

ergonic (energy-requiring) synthesis of the biological energy carrier, adenosine triphosphate (Schink, 1997; Hoehler, 2004). If the Gibbs energy requirement is met, metabolism using that energy source is possible. Theoretical and observational work place this requirement in the range of –10 to –20 kJ mol<sup>-1</sup> (Schink, 1997; Hoehler et al., 2001), and this provides a quantitative basis for evaluating potential redox energy sources for life. Biology is also heavily influenced by the flux of energy (how much energy through time), as life requires energy not only to construct new biomass, but also to maintain it through time (Tijhuis et al., 1993; Hoehler and Jørgensen, 2013). The biosynthetic (biomass-building) energy requirement is quite well quantified in terran biology, varying within an order of magnitude as an understood function of metabolic and biochemical specifics (e.g., McCollom and Amend, 2005; Thauer et al., 2008). This offers a means of equating energy fluxes with the amount of new biological material (e.g., cells, biosignatures, etc.) that can be created through time, even on global scales. The energy required to maintain existing biomass (“maintenance energy”) is well understood on theoretical grounds, but attempts to quantify it yield values that range over several orders of magnitude [10<sup>-19</sup>–10<sup>-13</sup> kJ cell<sup>-1</sup> d<sup>-1</sup> (Hoehler and Jørgensen, 2013, and references therein)]. Comparing maintenance energy requirements to planetary energy flux (see below) constrains the size of a biosphere that could be supported on a given world.

Compositional data can bear directly on what redox couples may exist and whether they offer sufficient Gibbs energy change to satisfy biological requirements. In particular, INMS measurements of the plume composition have been used to constrain the abundance of all products and reactants in the known terran metabolism methanogenesis, i.e., based on the reaction CO<sub>2</sub> + 4H<sub>2</sub> → CH<sub>4</sub> + 2H<sub>2</sub>O. Using these data, Waite et al. (2017) calculated the Gibbs energy change for methanogenesis,  $\Delta G_{\text{mp}}$ , as a function of pH (Fig. 8). The calculations suggest that H<sub>2</sub>-based methanogenesis would

occur with  $\Delta G_{\text{mp}} -120$  to  $-45$  kJ mol<sup>-1</sup> in the pH range of 9–11, levels that are both thermodynamically favorable ( $\Delta G_{\text{mp}} < 0$ ) and bioenergetically favorable ( $\Delta G_{\text{mp}} < -10$  to  $-20$  kJ mol<sup>-1</sup>).

It is more difficult to constrain energy flux on the basis of compositional data. However, this important parameter determines how large and productive, and thus how potentially detectable, a biosphere could be. Estimates of energy flux have generally considered the flux of the reductant, hydrogen (denoted here as  $J_{\text{H}_2}$ ), either from serpentinization (Vance *et al.*, 2016; Steel *et al.*, 2017; Taubner *et al.*, 2018) or radiolysis (Bouquet *et al.*, 2017) within the rocky core, into an ocean containing an excess of the oxidant, CO<sub>2</sub>. The energy potentially available by virtue of this flux is then  $(J_{\text{H}_2}/4) \times \Delta G_{\text{mp}}$ . The factor 4 accounts for the 4:1 stoichiometry of H<sub>2</sub>:CH<sub>4</sub> in the methanogenesis reaction, given that  $\Delta G_{\text{mp}}$  is typically expressed per mole of methane.

The observed H<sub>2</sub>:H<sub>2</sub>O mixing ratio in the plume volatiles indicates that H<sub>2</sub> is being lost from the moon itself at a rate of  $1\text{--}5 \times 10^9$  mol yr<sup>-1</sup> (Waite *et al.*, 2017), but this need not represent the present flux of H<sub>2</sub> into the ocean from the core. Instead, it serves to indicate that the ocean contains abundant H<sub>2</sub> — suggesting a substantive time-integrated  $J_{\text{H}_2}$  — and, combined with constraints on pH, supports the hypothesis that serpentinization has served, or is presently serving, as a source of H<sub>2</sub>. Efforts to constrain  $J_{\text{H}_2}$  thus depend on modeling the rate of serpentinization of the silicate core of Enceladus, with several approaches compared in Table 5:

1. Vance *et al.* (2016) calculated the  $J_{\text{H}_2}$  that would result from complete serpentinization of the silicate core at a continuous rate over the full age of the solar system. This estimate can be considered an upper-limit average if Enceladus' ocean has an age comparable to the age of the solar system, because it assumes full reaction of the silicate crust and also that H<sub>2</sub> production per unit of silicate rock is maximal in stoichiometric terms, whereas thermodynamic modeling indicates that H<sub>2</sub> yield per unit rock during ser-

pentization can vary more than 10-fold as a function of reaction temperature (McCollom and Bach, 2009). However, full reaction over the course of a shorter lifetime for Enceladus' ocean would yield correspondingly higher  $J_{\text{H}_2}$ .

2. Steel *et al.* (2017) used (a) a heat flow model to estimate rates of hydrothermal fluid venting, with assumed vent fluid H<sub>2</sub> concentrations corresponding to those of serpentinizing systems on Earth, and (b) a model that assumes H<sub>2</sub> production is limited by the rate of exposure of fresh mineral surfaces to water, and determines that exposure rate as a function of the propagation of fractures through the crust as it cools (Vance *et al.*, 2016).  $J_{\text{H}_2}$  calculated via the fracture model was within the range of  $J_{\text{H}_2}$  determined via the heat flow model.

3. Taubner *et al.* (2018) modified the fracture-based modeling approach to account for potentially slow dissolution of minerals at newly produced fracture surfaces, which could serve to limit H<sub>2</sub> production to lower rates.

These approaches yield estimates of  $J_{\text{H}_2}$  that vary over 5 orders of magnitude (Table 5). For completeness, it should be noted that ongoing radioactive decay within the silicate crust can generate both H<sub>2</sub> and oxidants (e.g., H<sub>2</sub>O<sub>2</sub>). Bouquet *et al.* (2017) calculate that this process could augment  $J_{\text{H}_2}$  from serpentinization [relative to, e.g., the results of Steel *et al.* (2017)] by as much as 30%, with results highly dependent on assumed grain size and porosity within the core.

Taubner *et al.* (2018) used  $J_{\text{H}_2}$  to estimate global rates of biomass production and Steel *et al.* (2017) estimated both global biomass production and bulk ocean average cell abundance. Biomass production estimates differ to an even larger extent than do the corresponding estimates of  $J_{\text{H}_2}$ , owing to differing approaches in the energy-biomass conversion. Notably, despite this large range, even the highest cell densities predicted for the Enceladus ocean are about 1000-fold lower than those typical of Earth's ocean [ $10^6$  cells cm<sup>-3</sup> (Watson *et al.*, 1977)], as would be expected for a more energy-constrained system.

TABLE 5. Estimates of energy flux and biological potential in Enceladus' interior.

	$J_{\text{H}_2}$ (mol s <sup>-1</sup> )	$J_{\text{Energy}}$ (W)	Biosynthesis (kg yr <sup>-1</sup> )	Cell abundance (cells cm <sup>-3</sup> ) <sup>§</sup>
Vance <i>et al.</i> (2016)*	96 <sup>†</sup>			
		$1.1 \times 10^6\text{--}2.9 \times 10^6$	$9.9 \times 10^5\text{--}5.4 \times 10^6$	0.6–890
Steel <i>et al.</i> (2017)*	0.6–34			
		$6.1 \times 10^3\text{--}1.9 \times 10^6$	$4 \times 10^4\text{--}2 \times 10^6$	80–4250
			$6.1 \times 10^3\text{--}1.9 \times 10^6$	0.004–340
Taubner <i>et al.</i> (2018)*	0.0009–0.013 <sup>†</sup>			
			12.6–162 <sup>‡</sup>	
		10.1–390	9.2–738	$6 \times 10^{-6}\text{--}0.12$

\* Values in upper panel (gray) were reported in the indicated paper. Values in the lower panel are recalculated based on reported  $J_{\text{H}_2}$ , and assumed values as follows:  $\Delta G_{\text{mp}} = -120$  to  $-45$  kJ (mol CH<sub>4</sub>)<sup>-1</sup> (Waite *et al.*, 2017); methanogen biomass yield =  $1.3\text{--}7.2$  (g dry biomass)<sup>-1</sup>(mol CH<sub>4</sub>)<sup>-1</sup> (Thauer *et al.*, 2008); maintenance energy =  $1.2 \times 10^{-19}$  to  $6 \times 10^{-17}$  W cell<sup>-1</sup> (Tijhuis *et al.*, 1993; Hoehler and Jørgensen, 2013); average cell mass =  $2 \times 10^{-14}$  g (Fagerbakke *et al.*, 1996).

<sup>†</sup> Converted from values reported in units of mol yr<sup>-1</sup>.

<sup>‡</sup> Converted from values reported in units of C nmol g<sup>-1</sup> L<sup>-1</sup> yr<sup>-1</sup>.

<sup>§</sup> Calculated as a bulk ocean average, assuming an ocean volume of  $2.7 \times 10^{16}$  m<sup>3</sup> (Steel *et al.*, 2017).

To compare the implications of the three models for biospheric size and productivity on a common basis, we used the values of  $J_{H_2}$  reported in each study to (re) calculate global energy flux, global biomass production rate, and standing cell abundance (Table 5). For each, the values presented reflect the compound uncertainty in  $J_{H_2}$ ,  $\Delta G_{mp}$ , biosynthesis yield for methanogenesis, and cellular maintenance energy. The results of Table 5 demonstrate the presently large uncertainty in estimating biological potential for Enceladus. This is true even within a single study, and particularly regarding the potential of a system to support a standing biosphere. For example, *Steel et al.* (2017) estimated bulk ocean cell abundances of 80–4250 cells  $cm^{-3}$  by assuming an average cell lifetime of 1000 yr but no energetic cost for cell maintenance. The recalculated values, which include maintenance energy costs as observed in terran organisms, are 1–3 orders of magnitude lower and span an overall range of nearly 5 orders of magnitude. Better constrained estimates of both planetary energy flux and biomass-energy relations would help in narrowing the presently large range of possibility, as required to inform the strategies and measurement requirements of a search for evidence of life. This is an important area for advancement in further observations of Enceladus.

### 5.3. Unused Energy?

Exclusive of uncertainties in energy flux, constraints on plume composition indicate that energy is available in a known terran metabolism, methanogenesis, at levels that would satisfy terran Gibbs energy requirements (*Waite et al.*, 2018). Does the presence of such unused energy imply that no life is present to use it? This is a possibility, but the alternative cannot be ruled out.

“Unused energy” in plume chemistry could be consistent with an inhabited world if the plume sample fluids that have a residence time (the length of time the fluids are in the plume) that is short in comparison to the timescales associated with microbial growth and substrate utilization. The bulk ocean is estimated to have a residence time of about 200 m.y. with respect to recycling through warm crust and a mixing rate of kiloyears (*Steel et al.*, 2017), both much longer than the timescales associated with microbial growth. However, it has been suggested that buoyant vent fluid could be transported to the base of the ice shell in relatively coherent columns on a timescale of months (*Steel et al.*, 2017), which might be too short to allow for microbes to colonize and fully deplete available energy sources. If plume materials directly sampled such fluid columns, they could contain unused energy even on an inhabited world. This would also imply that plume measurements are reflective of vent fluid rather than bulk ocean chemistry.

Alternatively, physical or chemical factors might inhibit the origin or current presence of life, despite the presence of energy that could be used by biology. *Taubner et al.* (2018) addressed the sensitivity of methanogen growth and activity to a range of conditions and potentially inhibitory

substances that are associated with the Enceladus ocean. Those experiments demonstrated activity of at least some methanogens across much of the range of imposed conditions. Importantly, however, the pH of these experiments decreased due to the presence of  $CO_2$  at high pressure to a range of pH 5–7, whereas Enceladus’ ocean is thought to have an alkaline pH (*Glein et al.*, 2015; *Waite et al.*, 2017). Alkaline pH at the high end of the currently predicted range of 9–11 (*Glein et al.*, 2018) could prove inhibitory to biological growth or activity, as methanogen growth has thus far not been observed above pH 10.2 (*Taubner et al.*, 2015) and likewise could frustrate the formation of hydrolyzable polymers in a prebiotic stage of chemistry. High pH also decreases the solubilities of transition metals (Fe, Ni) that are typically utilized to catalyze key biochemical reactions in cells (i.e., in enzymes). However, on Earth this decreased solubility leads to precipitation of chimneys (i.e., Lost City) on the seafloor that concentrate minerals and focus redox/chemical gradients, potentially acting as incubators for biochemistry leading to life (*Barge and White*, 2017, and references therein). Further experimental and theoretical work is needed to fully understand the implications of pH and other factors on the energy budget of Enceladus.

### 5.4. Summary of Enceladus’ Astrobiological Potential

Relative to the requirements and tolerances of modern terran life, Enceladus appears to be habitable. Qualitatively, it provides solvent, a supply of the biogenic elements, redox chemical energy, and physicochemical conditions in a range tolerated by at least some terran organisms. The impact of a potentially alkaline ocean pH on both the origin and modern-day activity of life remains as a key factor to understand. Quantitatively, any potential biosphere on Enceladus seems more likely to be limited by availability of energy than of the biogenic elements, with the caveat that the possibility for phosphorus limitation remains to be extensively considered. Present estimates of energy flux range over orders of magnitude, which affects the detectability of any biosphere, and how best to search for it. Whether or not Enceladus is, in fact, inhabited remains to be determined by future missions.

## 6. LIFE DETECTION ON ENCELADUS: BIOSIGNATURES AND MEASUREMENT REQUIREMENTS

Enceladus, which appears to meet current requirements for habitability, may hold the answer to one of the most profound questions: Does life exist elsewhere? Its ocean material can be accessed through the plume, circumventing the technological and planetary protection (see the chapter by Rummel in this volume) challenges of drilling through the icy crust.

Despite the ready sample access, a definitive answer to the life question will undoubtedly pose a significant challenge. Careful design of experiments, built upon the

knowledge from the Cassini mission, may get us closer to eliminating abiotic hypotheses for the presence of potential biosignatures (Neveu *et al.*, 2018). A key step in this process is identifying biosignatures appropriate for this particular environment and where they might be found.

### 6.1. Biosignatures: Progress and Potential Pitfalls

Since the first “life” experiments on the Viking landers sent to Mars (see the chapter by Davila *et al.* in this volume), scientists and engineers have worked to design the most straightforward experiments to search for life while being as agnostic as possible to what that life might be. A few relevant biosignatures are discussed below, along with unique considerations for their detection in the Enceladus environment. While not a comprehensive list, the biosignatures described here illustrate the diverse approaches to life detection, as well as their potential weaknesses.

**6.1.1. Amino acids.** Amino acids, the building blocks of proteins, may serve as an excellent biosignature, given a few caveats. Amino acids can be generated both biotically and abiotically. They are commonly found in meteorites and are most likely present on Enceladus either due to primordial accretion (i.e., they were present in the carbonaceous chondrites from which Enceladus formed) and/or due to geochemical synthesis via serpentinization (Truong *et al.*, 2019). Biotic and abiotic amino acids can be distinguished in two ways: (1) enantiomeric excess (defined below) and (2) relative abundances compared to glycine.

Nearly all amino acids (except glycine) are chiral molecules: They and their mirror images are not superimposable (Berg *et al.*, 2012a). This means each amino acid has two forms called enantiomers, referred to as “L” or “D” based on the direction each rotates in plane-polarized light (“L” for levorotatory or counterclockwise, “D” for dextrorotatory or clockwise). In biochemistry, substituting a “D” for an “L” amino acid could cause a protein to fold differently, or prevent binding of an enzyme to a substrate. Thus, presumably to keep biological reactions simple, biology exhibits homochirality: All life as we know it uses only “L” amino acids (the question of why “L” and not “D” is debated). Importantly, most abiotic reactions do not exhibit chiral selectivity: Abiotic amino acids are an equal (50/50) mixture of “L” and “D” enantiomers. This is referred to as a racemic mixture, and any process that causes erasure of enantiomeric excess (a greater percentage of the “L” or “D” form relative to the other) is termed racemization.

Thus, an excess of either enantiomer would provide evidence against an abiotic source (Summons *et al.*, 2008, and references therein), and an excess of “D” amino acids would also be strong evidence that this life had evolved independently of life on Earth (McKay, 2004). However, accurate detection of enantiomeric excess can be confounded by an abundance of abiotic amino acids and racemization over time. Racemization in the Enceladus ocean may take place in just  $10^4$ – $10^7$  yr (Steel *et al.*, 2017), so even biological activity that is recent in geological terms may not leave

a detectable signal. Alternatively, if indeed an enantiomeric excess is detected at Enceladus, it would be strong evidence of a biosignature for recent life (within the last 10 m.y.).

Evidence from enantiomeric excess might be complemented by amino acid patterns. Abiotic generation of amino acids produces distributions consistent with thermodynamics: The simplest amino acids (glycine, alanine) are much more abundant than those that are larger or more complex. This is seen in meteorites, where glycine is typically more abundant than other amino acids by  $\sim 2$  orders of magnitude (Cronin and Pizzarello, 1983; Higgs and Pudritz, 2009). In contrast, life requires more complex amino acids to induce protein folding motifs and create binding sites for metals and other substrates, essentially to form and operate the “molecular machinery” of life. Thus, environments influenced by biology tend to have amino acid patterns where serine, tyrosine, and other relatively complex amino acids are as abundant as glycine (Davila and McKay, 2014; McKay, 2004; Glavin *et al.*, 2010; Creamer *et al.*, 2017; Cable *et al.*, 2016).

However, with comparisons of amino acid abundances or mole fractions, abiotic production and destruction rates must be considered. Abiotic synthesis of the aromatic amino acid tryptophan was recently confirmed in clay-forming hydrothermal alteration of oceanic rocks (Fe-rich saponite) at depth beneath the Mid-Atlantic Ridge (Menez *et al.*, 2018), possibly ruling out this amino acid as a biosignature without a deeper understanding of the rates of abiotic production. Truong *et al.* (2019) calculated that the amino acids aspartic acid and threonine are particularly sensitive to decomposition in the Enceladus ocean, or the ocean of any hydrothermally active ocean world. While this implies that the ratio of these two amino acids to glycine might not have utility over longer timescales, it does provide another potential biosignature: Any aspartic acid or threonine detected in Enceladus’ ocean must have been produced recently (within 1 m.y.) and cannot be primordial. Based on the model of Truong *et al.* (2019), any amino acids found at concentrations greater than 1 nM in the Enceladus ocean would indicate recent production via geochemical or biotic pathways; such concentrations could not be achieved with replenishment by cometary impact.

Simple amino acids probably exist as zwitterions (a molecule having separate positively and negatively charged groups, and thus a net neutral charge) or singly charged ions in the Enceladus ocean, depending on the equilibrium acid dissociation constant ( $pK_a$ ) of their side-chain [e.g., the side chain of arginine is charged even at pH 10 (Fitch *et al.*, 2015)]. Those that have charge will probably bind to cations like  $Na^+$ ; due to this and their relatively low volatilities, amino acids are most likely to be found in the grains of the Enceladus plume as opposed to the gas (Glein *et al.*, 2015) (section 3). This would also be true for proteins or protein fragments (polypeptides).

**6.1.2. Lipids.** A similar diagnostic test of life can be found in another set of molecules found in all known forms of life: lipids. These molecules typically have long, nonpolar, hydrophobic carbon chains that self-assemble



into micelles and lipid bilayers, creating cell membranes. The carbon distribution in lipids used by life follows patterns. In bacteria and eukaryotes, lipid synthesis involves building chains two carbons at a time, yielding an excess of carbon chains of even length. In archaea, lipid chains are synthesized five carbons at a time (Berg et al., 2012b). This is in stark contrast to abiotic synthesis of carbon chains (via Fischer-Tropsch-type reactions), which typically produces a standard distribution (Anderson-Schulz-Flory) of chain lengths with no addition pattern (Dorn et al., 2011; Fortsch et al., 2015). Thus, the detection of a pattern of repeating subunits in carbon chains of lipids may be a universal biosignature (Summons et al., 2008; Georgiou and Deamer, 2014; Parnell et al., 2007; Cable et al., 2016). Furthermore, methanogens produce distinct ether lipids and isoprenoid hydrocarbons that could supplement the lipid pattern biosignature on Enceladus (Taubner et al., 2018).

As with the amino acid biosignature, a thorough understanding of lipid degradation in the Enceladus environment is needed. Fortunately, degradation processes on Earth have been demonstrated to preserve the pattern (Moldowan et al., 1985). As in the case of the amino acids, lipids and other long-chain carbon molecules are likely to be present in the plume grains, as they are not volatile enough to reach the gas phase. The detection of high-mass organic cations in the plume grains (Postberg et al., 2018) may support this assessment.

**6.1.3. Small molecules indicative of active biochemistry.** Due to the alkalinity of the Enceladus ocean, hydroxide ions (OH<sup>-</sup>) are likely to be abundant, opening up the potential for base-catalyzed reactions to influence the chemistry of organics in the ocean (Glein et al., 2015). Molecules such as urea, nitriles, and acetyl thioesters, which hydrolyze rapidly under basic conditions, could serve as indicators of active biochemistry: If they are detected in such an environment, they must be produced at the present day. As with the biosignatures discussed above, evidence of these species is likely to be found frozen in the plume grains if they carry a charge, although neutral volatile reaction intermediates or products, such as amines, may be detectable in the plume gas.

**6.1.4. Large molecules.** Large, information-carrying macromolecules such as proteins, RNA, and DNA can serve as informative biosignatures. However, these are very Earth-life-centric. A more agnostic biosignature was proposed by Benner (2017): the presence of polymers with repeating charges in their backbones (the connecting chain in a polymer, also known as the main chain). These repeating charges force interstrand interactions in the polymer, and make it more likely to adopt an extended shape suitable for templating (neutral polymers tend to fold) to enable copying/replication of information. Repeating charges also ensure that the entire polymer will have similar physical properties, dominated by these charge interactions, even when the informational content of that polymer changes. Such large molecules, if they exist on Enceladus, could be present in the plume grains, either the salt-rich Type III or organic-rich

Type II grains (section 2), depending on whether they are free-floating molecules or entrained within hydrophobic cells or cell debris (next section).

**6.1.5. Cells and cell assemblages.** The chemical energy available in the ocean of Enceladus may be able to support cell densities up to  $\sim 10^3$  cells cm<sup>-3</sup>. However, this value is highly model-dependent (see Table 5) and represents a bulk ocean average; cell densities could be higher in certain regions (i.e., near vents). Cells could be ejected in the plume (Porco et al., 2017), frozen within grains of sufficient size (most unicellular organisms on Earth are 0.2  $\mu$ m or larger) (Europa Lander Mission Concept Team, 2016, and references therein). The detection of cells within a plume grain depends on many factors, such as concentration mechanisms (sections 2 and 6.1.7), how the grains are sampled [capture above  $\sim 2$  km s<sup>-1</sup> can destroy cells, but encasing cells within ice provides protection (Aksyonov and Williams, 2001; Burchell et al., 2014; Porco et al., 2017)], and where the grains are sampled (large grains do not reach high altitudes; section 2).

More complex assemblages of microorganisms, such as biofilms or microbial mats, might also occur in areas where energy or nutrients are concentrated, such as at hydrothermal vents or the ice-ocean interface (Russell et al., 2017). In the latter case, assuming they are preserved in the ice shell, evidence of life may be detectable *in situ* with microscopic or spectroscopic techniques (Gleeson et al., 2012; Storrie-Lombardi and Sattler, 2009) or remotely via high-resolution imagery or key absorption features in the visible range if the deposit is substantial [water-ice tends to mask microbial absorptions in the near-infrared (Poch et al., 2017)]. Sublimation may concentrate less-volatile biosignatures and improve detectability, in particular in Sun-exposed surface materials.

**6.1.6. Biosignature concentration and preservation.** Enceladus may host some unique conditions that could enhance the concentration and/or residence time of biosignatures. Organic material may become concentrated at the ocean-ice interface, similar to the formation of sea-spray aerosols on Earth, which can provide up to 1000-fold organic enrichment compared to the bulk ocean concentration (section 2). Moreover, any volatile exsolution leading to bubbles rising through the water column could scavenge organic material, including microorganisms, which would tend to attach to the bubble surface (Porco et al., 2017). This process is most efficient with hydrophobic molecules and surfactants (which have a hydrophilic head and a hydrophobic tail), and has been shown to increase organic and microbial concentrations by orders of magnitude on Earth (Carlucci and Williams, 1965; Blanchard and Syzdek, 1972). However, this may not occur if turbulent mixing is occurring in the fractures. It is not clear whether these two enrichment processes are complementary or mutually exclusive, but if they occur on Enceladus, the potential for detecting organic biosignatures in the plume is much higher than may be expected based on estimates of bulk concentrations in the ocean alone.

The alkaline pH of the ocean, the nondetection of molecular oxygen by the Cassini Ultra Violet Imaging Spectrograph (UVIS) (Hansen *et al.*, 2005), and the lack of abundant sulfate in the plume (Glein *et al.*, 2015) all suggest that delivery of strong oxidants such as O<sub>2</sub> from the surface to the ocean of Enceladus has not been significant. In Earth's oceans, in the absence of O<sub>2</sub>, organic matter is degraded much more slowly (e.g., Cowie *et al.*, 1995). Anoxia in the Enceladus ocean may therefore improve the preservation of organic material, including any biosignatures. However, Glein *et al.* (2015) note that the absence of sulfate could also be explained by robust oxidant delivery and rapid sulfate reduction by life, if enough organisms and reductants (e.g., H<sub>2</sub> from serpentinization) are present. A future mission to Enceladus may help resolve these questions.

## 6.2. Measurement Requirements

Cassini's instruments were designed to only interrogate simple molecules, because more complex compounds were unexpected in the Saturn system when Cassini was designed. The next missions to reach the Saturn system will undoubtedly have more advanced instrumentation. These instruments will likely be able to identify complex organic molecules, and hopefully distinguish biotic from abiotic compounds.

A path to life detection on an ocean world such as Enceladus is still in development (Fig. 9). Sherwood (2016) proposed three basic steps: (1) validation of habitability, (2) detection of biosignatures, and (3) confirmation of life. Arguably, the first step has been achieved at Enceladus with the Cassini mission. This mission has also helped constrain measurement requirements to achieve the second.

Many Enceladus mission concepts have been proposed at various levels of maturity (Sherwood, 2016). Architectures include a plume fly-through/orbiter, lander, sample return, fracture explorer/climber, and submersible. Measurement requirements for these mission concepts vary

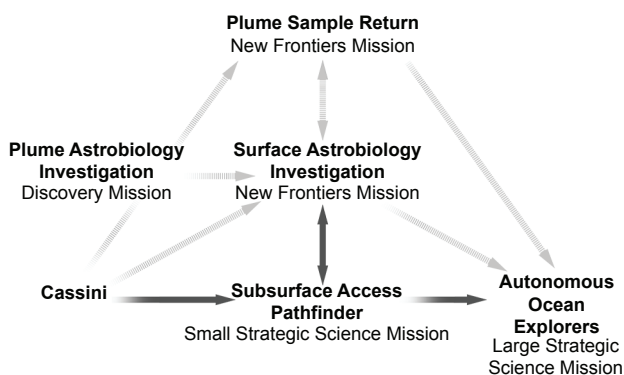


**Fig. 9.** Possible paths of investigation to search for life on Enceladus. Some paths may involve different mission classes (i.e., “New Frontiers” or “Strategic Science” missions in the NASA denomination). Dashed arrows indicate orbital/flyby/surface missions; solid arrows require subsurface access. Modified from Sherwood (2016).

based on which environment is targeted: the plume, the surface, or the ocean.

**6.2.1. In situ plume sampling.** Cassini mission operations demonstrated that plume gas and grains could be successfully sampled *in situ* at speeds of 8–18 km s<sup>-1</sup> (these speeds are of the spacecraft relative to Enceladus; the plume velocity in the direction of the fly-through is negligible in comparison). A future plume fly-through mission concept could build on this work, using instruments sensitive to the energy of hypervelocity impacts [4–6 km s<sup>-1</sup> has been reported as the optimal velocity range for detection of biomolecules such as amino acids, fatty acids, and peptides; at these speeds, biomolecules entrained in ice grains are ionized upon impact with minimal fragmentation, allowing analysis via mass spectrometry (Jaramillo-Botero *et al.*, 2012; Klenner *et al.*, 2020)]. Hypervelocity capture of cells is also possible (section 6.1.6), although more laboratory work and modeling would help characterize the relationship between capture speed and cell/ice ratio in preserving cell integrity.

An Enceladus orbiter could achieve fly-through speeds <1 km s<sup>-1</sup>, enabling soft capture of grains for analysis. However, planetary protection requirements for the disposal of such a spacecraft are critical, as a significant amount of fuel would be needed to leave Enceladus orbit and impact a body of less astrobiological potential.

Given the half-angle (the angle from normal/perpendicular to the surface that defines the plume spread as it leaves the source) of 15° assumed for most plume models (Hansen *et al.*, 2008, Kempf *et al.*, 2010) and the distance between the tiger stripes, the material from the jets and curtains diffuses into a single plume at an altitude of ~45 km. Any future mission targeting the Enceladus plume would therefore have a high probability of collecting plume material in a flyby over the south polar terrain at this altitude, irrespective of whether the ground track is directly over an identified discrete jet.

A sample return architecture is also possible; analyses of returned samples are complementary to *in situ* measurements. Returned samples lack field environmental context and can undergo changes during sampling, caching, the return cruise, reentry, recovery, handling, and storage. However, sample return analyses are uniquely suited to addressing the need for complex, path-dependent analyses (Tsou *et al.*, 2012; McKay *et al.*, 2014). They therefore provide the ability to adapt to unexpected findings, which have been the hallmark of past searches for biosignatures (e.g., Klein, 1978; McKay *et al.*, 1996). Moreover, returned samples can be analyzed with the entire set of analytical techniques available on Earth, some of which cannot be flown, and none of which can be flown at a level of performance rivaling that achievable on Earth. Finally, samples can be archived for future analysis using techniques that we may not have conceived of yet.

Biosignature concentrations in the plume can be estimated based on (1) their predicted concentration in the ocean [i.e., 0.01–90 μmol (kg H<sub>2</sub>O)<sup>-1</sup> for amino acids (Steel

et al., 2017)], (2) possible concentration before/during ejection (bubble scrubbing, enrichment via sea spray aerosol from a boundary layer, sublimation, etc.), and (3) models of plume gas and grain density over the fly-through sampling trajectory. Evidence suggests that the concentration of organic material in the plume is above detection limits of modern instruments ready or soon-to-be ready for flight: CDA onboard Cassini, an instrument built more than 20 yr ago, detected organic macromolecular compounds at concentrations well above its limit of detection, but did not have the mass resolution to identify their specific elemental compositions (Postberg et al., 2018). For trace species, large collection apertures, cryotrapping, and/or multiple plume fly-throughs may be employed to obtain sufficient sample to meet instrument performance requirements. Other architectures such as a “plume hoverer” could also improve plume grain collection efficiency.

**6.2.2. Sampling the surface.** A lander to Enceladus, while much more complex than an orbital or fly-through architecture, offers unique advantages. A landed mission to the tiger stripes could access the largest grains emitted from the plume, since 68–93% of Enceladus plume particles fall back to the surface, including the largest grains more likely to contain whole cells (Porco et al., 2017). A lander could also collect significantly greater sample volume than a plume fly-through mission could on a single pass.

However, significant obstacles exist for a lander. Planetary protection requirements must be considered, especially if the landed mission is powered by radioisotope thermoelectric generators. The probability of inadvertently melting through the ice, or any other mechanism by which microbial hitchhikers from Earth could reach the ocean, must be reduced to below  $10^{-4}$  (National Research Council, 2012). In addition, a lander would be more costly, requiring a larger-class mission (Sherwood, 2016). Recent science and technology developments such as the Europa Lander mission concept (Europa Lander Mission Concept Team, 2016) and other programs, including the Concepts for Ocean worlds Life Detection Technology (COLDTech) and the Instrument Concepts for Exploration of Europa 2 (ICEE-2), could be leveraged to make such a mission possible in the coming years or decades. In addition, complementary efforts to these NASA programs are being undertaken worldwide.

**6.2.3. Reaching the ocean.** While not explicitly needed to answer the life question, absolute confirmation of microbial communities thriving near hydrothermal vents at the seafloor of Enceladus (or elsewhere in the ocean) would require direct access to the ocean. To achieve this, significant technological advancements are needed, ranging from melt probes or descent vehicles capable of navigating through the plume vents, to communication strategies to reach through  $\geq 1$  km of ice, to submersibles capable of autonomous navigation and with the appropriate scientific payload (Sherwood, 2016). Planetary protection requirements for such a mission would be appropriately more strict than for landers or plume flyby architectures. Much work is underway, including

funded programs in the U.S. and internationally, such as the Scientific Exploration of Subsurface Access Mechanism for Europa (SESAME) program, that would pave the way for exploration of many worlds in addition to Enceladus such as Europa, Titan, Ganymede, or perhaps even Triton.

## 7. OUTSTANDING QUESTIONS AND FURTHER READING

### 7.1. Outstanding Questions

Enceladus is one of the best places to look for life beyond Earth. Recognizing evidence of life in this moon, or interpreting the lack of life, will require answers to several outstanding questions. The list below covers three key areas of focus: the longevity of habitable conditions inside Enceladus, the modifications that material from possible subsurface habitats may undergo between its provenance and sampling locations, and the broader question of what evidence is sufficient to claim life detection.

*How old is Enceladus?* Much headway has been made in tackling this question in the past few years (Canup, 2010; Charnoz et al., 2011; Asphaug and Reufer, 2013; Cuk, 2016; Lainey et al., 2017). These studies have considerably broadened the fan of hypotheses for the origin of Enceladus and Saturn’s other mid-sized moons. These new ideas on how moon systems might form and evolve, while exciting, show just how little is known about the history of these systems.

*Can Enceladus’ starting materials be better constrained?* What ocean and core compositions result from starting compositions compatible with formation scenarios? Do they match measurements of surface and ejected material?

*How does tidal heating work on Enceladus?* How is it partitioned between the core, ocean, and ice shell? Can a better understanding of Enceladus inform these processes on other ocean worlds?

*How long has the ocean existed?* Accurate estimates by forward modeling require coupling detailed geophysical and orbital models that must be used to run simulations with about  $10^{14}$  time steps (a hundred times a day over 4.5 b.y.). This is currently unachievable in any reasonable amount of time. Are there simplified modeling or observational means of constraining the age of the ocean?

*To what extent have water and rock interacted?* Is the core solid rock, loose sand and/or mud, or both? How extensive is the water-rock interface?

*How close to chemical equilibrium is Enceladus?* In principle, detailed forward modeling or experiments seeking to mimic mass spectrometric data collected by Cassini instruments could place tight constraints on the chemistry of Enceladus’ water-rock interactions. One confounding factor is the potential for chemical fractionations as material is erupted and vented out, limiting for now robust compositional interpretations to refractory solids (Postberg et al., 2011; Hsu et al., 2015; Sekine et al., 2015). In particular, detailed investigation of how exsolution and



eruptive processes might affect H<sub>2</sub> abundances in the plume would be very informative, given its diagnostic power on the extent, progress, and speed of water-rock reactions and its use as a metabolic substrate by terran life. Studies of surface oxidant production and delivery to the ocean would constrain the oxidant supply.

*How long has the plume been active?* We know that the plume is at least decades old due to the presence of the E ring, but how much older is it? If it is episodic, what are its primary drivers?

*How much is material modified or concentrated as it moves from the ocean to the plume?* What are the characteristics of the conduits linking the ocean to the surface (e.g., aspect ratio, branching, chambers, wall roughness, lifetime), and how do these affect fluid ascent? Are the relative abundances of the chemical species seen in the plume equivalent to what is in the ocean, or have these ratios been modified en route? Is organic enrichment taking place? How much chemistry is happening in the vents?

*How long has Enceladus been habitable?* How much time has life had to arise on Enceladus? Is that time sufficient? If not, how far has prebiotic chemistry progressed? Will conditions persist long enough for life to emerge in the future? If life has just emerged on Enceladus, but has not yet become fully established (reached biological saturation based on nutrient availability), would any biosignatures still be above detection limits?

*What would constitute convincing evidence of life on Enceladus?* Would two independent biosignatures be enough? Would the scientific community be more easily convinced than the general public? Would seeing a motile cell or a squid be needed to settle any debate?

In the end, either discovering life on Enceladus or constraining its absence to below a biomass threshold would have profound implications for our understanding of life in a cosmic context. If life is present on Enceladus, it most likely emerged separately from life on Earth, owing to the low likelihood of material transfer between the two worlds (Worth *et al.*, 2013). This would imply that the emergence of life on habitable worlds is common, i.e., the  $f_l$  factor in the Drake equation (Drake, 2003) is high. Conversely, the absence of life on Enceladus seems impossible to ascertain unless each square micrometer of its material is analyzed. However, constraining the absence of biomass to below a threshold consistent with Enceladus' habitability would provide a solid example of an environment in which life is limited, bringing about a need to reconsider requirements for life in such environments. Either way, exploring Enceladus could revolutionize our understanding of how life works.

## 7.2. Further Reading

- Spencer J. R. and Nimmo F. (2013) Enceladus: An active ice world in the Saturn system. *Annu. Rev. Earth Planet. Sci.*, 41, 693–717.
- Dougherty M., Esposito L., and Krimigis S., eds. (2009) *Saturn from Cassini-Huygens*. Springer, Berlin.
- Schenk P. M., Clark R. N., Howett C. J. A., Verbiscer A. J., and Waite J. H., eds. (2018) *Enceladus and the Icy Moons of Saturn*. Univ. of Arizona, Tucson.
- Hoehler T. M. and Jørgensen B. B. (2013) Microbial life under extreme energy limitation. *Nature Rev. Microbiol.*, 11, 83–94.
- The Saturn System: Through the Eyes of Cassini* (2017) E-book, National Aeronautics and Space Administration (NASA)/Lunar and Planetary Institute (LPI), available online at <https://www.nasa.gov/connect/ebooks/the-saturn-system.html>.
- Acknowledgments.** We thank everyone on the Cassini mission, without whom Enceladus would have remained a mystery out of reach. We also thank C. Glein and C. J. A. Howett for their thorough and very helpful reviews of this chapter. Some of this research was carried out at the Jet Propulsion Laboratory, California Institute of Technology, under a contract with the National Aeronautics and Space Administration. Government sponsorship acknowledged.

## REFERENCES

- Abrajano T. A., Sturchio N. C., Kennedy B. M., Lyon G. L., Muehlenbachs K., and Bohlke J. K. (1990) Geochemistry of reduced gas related to serpentinization of the Zambales ophiolite, Philippines. *Appl. Geochem.*, 5(5), 625–630, DOI: 10.1016/0883-2927(90)90060-I.
- Aksyonov S. A. and Williams P. (2001) Impact desolvation of electrosprayed microdroplets — a new ionization method for mass spectrometry of large biomolecules. *Rapid Commun. Mass Spectrom.*, 15, 2001–2006, DOI:10.1002/rcm.470
- Alexander C. M. O'D., Cody G. D., De Gregorio B. T., Nittler L. R., and Stroud R. M. (2017) The nature, origin and modification of insoluble organic matter in chondrites, the major source of Earth's C and N. *Chem. Erde-Geochem.*, 77(2), 227–256, DOI: 10.1016/j.chemer.2017.01.007.
- Alibert Y., Mousis O., and Benz W. (2005) Modeling the jovian subnebula. I. Thermodynamic conditions and migration of proto-satellites. *Astron. Astrophys.*, 439, 1205–1213.
- Anderson J. S., Rittle J., and Peters J. C. (2013) Catalytic conversion of nitrogen to ammonia by an iron model complex. *Nature*, 501(7465), 84–87, DOI: 10.1038/nature12435.
- Asphaug E. and Reufer A. (2013) Late origin of the Saturn system. *Icarus*, 223, 544–565, DOI: 10.1016/j.icarus.2012.12.009.
- Arnold H., Liuzzo L., and Simon S. (2019) Magnetic signatures of a plume at Europa during the Galileo E26 flyby. *Geophys. Res. Lett.*, 46, 1149–1157.
- Auzende A.-L., Pellenq R. J.-M., Devouard B., Baronnet A., and Grauby O. (2006) Atomistic calculations of structural and elastic properties of serpentine minerals: The case of lizardite. *Phys. Chem. Mineral.*, 33, 266–275, DOI: 10.1007/s00269-006-0078-x.
- Barge L. M. and White L. M. (2017) Experimentally testing hydrothermal vent origin of life on Enceladus and other icy/ocean worlds. *Astrobiology*, 17(9), 820–833.
- Barr A. C. and McKinnon W. B. (2007) Convection in ice I shells and mantles with self-consistent grain size. *J. Geophys. Res.*, 112, E02012, DOI: 10.1029/2006JE002781.
- Běhouňková M., Tobie G., Čadek O., Choblet G., Porco C., and Nimmo F. (2015) Timing of water plume eruptions on Enceladus explained by interior viscosity structure. *Nature Geosci.*, 8, 601–606, DOI: 10.1038/ngeo2475.
- Benner S. A. (2017) Detecting Darwinism from molecules in the Enceladus plumes, Jupiter's moons, and other planetary water lagoons. *Astrobiology*, 17(9), 840–851, DOI: 10.1089/ast.2016.1611.
- Berg J. M., Tymoczko J. L., and Stryer L. (2012a) Protein composition and structure. In *Biochemistry*, 7th edition. Freeman, New York. 1050 pp.
- Berg J. M., Tymoczko J. L., and Stryer L. (2012b) Fatty acid metabolism. In *Biochemistry*, 7th edition. Freeman, New York.



- 1050 pp.
- Beuthe M., Rivoldini A., and Trinh A. (2016) Enceladus's and Dione's floating ice shells supported by minimum stress isostasy. *Geophys. Res. Lett.*, *43*, 10088–10096, DOI: 10.1002/2016GL070650.
- Blanchard D. C. and Syzdek L. D. (1972) Concentration of bacteria in jet drops from bursting bubbles. *J. Geophys. Res.*, *77*, 5087–5099, DOI: 10.1029/JC077i027p05087.
- Bland M. T., Singer K. N., McKinnon W. B., and Schenk P. M. (2012) Enceladus' extreme heat flux as revealed by its relaxed craters. *Geophys. Res. Lett.*, *39*(17), L17204, DOI: 10.1029/2012GL052736.
- Bland P. A. and Travis B. J. (2017) Giant convecting mud balls of the early solar system. *Sci. Adv.*, *3*(7), e1602514, DOI: 10.1126/sciadv.1602514.
- Bockelée-Morvan D., Crovisier J., Mumma M. J., and Weaver H. A. (2004) The composition of cometary volatiles. In *Comets II* (M. C. Festou et al., eds.), Univ. of Arizona, Tucson.
- Bouquet A., Mousis O., Waite J. H., and Picaud S. (2015) Possible evidence for a methane source in Enceladus' ocean. *Geophys. Res. Lett.*, *42*, 1334–1339, DOI: 10.1002/2014GL063013.
- Bouquet A., Glein C. R., Wyrick D., and Waite J. H. (2017) Alternative energy: Production of H<sub>2</sub> by radiolysis of water in the rocky cores of icy bodies. *Astrophys. J. Lett.*, *840*, L8, DOI: 10.3847/2041-8213/a66d56.
- Brazelton W. J., Schrenk M. O., Kelley D. S., and Baross J. A. (2006) Methane- and sulfur-metabolizing microbial communities dominate the Lost City hydrothermal field ecosystem. *Appl. Environ. Microbiol.*, *72*, 6257–6270.
- Burchell M. J., Bowden S. A., Cole M., Price M. C., and Parnell J. (2014) Survival of organic materials in hypervelocity impacts of ice on sand, ice, and water in the laboratory. *Astrobiology*, *14*(6), 473–485.
- Burger M. H., Sittler E. C., Johnson R. E., Smith H. T., Tucker O. J., and Shematovich V. I. (2007) Understanding the escape of water from Enceladus. *J. Geophys. Res.*, *112*, A06219, DOI: 10.1029/2006JA012086.
- Burrows S. M., Ogunro O., Frossard A. A., Russell L. M., Rasch P. J., and Elliott S. M. (2014) A physically based framework for modeling the organic fractionation of sea spray aerosol from bubble film Langmuir equilibria. *Atmos. Chem. Phys.*, *14*, 13601–13629, DOI: 10.5194/acp-14-13601-2014.
- Cable M. L., Clark K., Lunine J. I., Postberg F., Reh K., Spilker L. J., and Waite J. H. (2016) Enceladus Life Finder: The search for life in a habitable moon. *IEEE Aerospace Conference*, Big Sky, Montana, 1–8, available online at <http://hdl.handle.net/2014/45905>.
- Cable M. L., Postberg F., Lang S. Q., Aluqihare L., Huber J., Clark B., Spilker L. J., and Lunine J. I. (2017) Mechanisms for enrichment of organics in the Enceladus plume. *Astrobiology Science Conference*, abstract #3639.
- Čadek O., Tobie G., Van Hoolst T., Massé M., Choblet G., Lefèvre A., Mitri G., Baland R.-M., Běhouňková M., Bourgeois O., and Trinh A. (2016) Enceladus's internal ocean and ice shell constrained from Cassini gravity, shape, and libration data. *Geophys. Res. Lett.*, *43*, 5633–5660, DOI: 10.1002/2016GL068634.
- Čadek O., Souček O., Běhouňková M., Choblet G., Tobie G., and Hron J. (2019) Long-term stability of Enceladus' uneven ice shell. *Icarus*, *319*, 476–484.
- Canup R. M. (2010) Origin of Saturn's rings and inner moons by mass removal from a lost Titan-sized satellite. *Nature*, *468*, 943–946, DOI: 10.1038/nature09661.
- Canup R. M. and Ward W. R. (2006) A common mass scaling for satellite systems of gaseous planets. *Nature*, *44*, 834–839, DOI: 10.1038/nature04860.
- Carlucci A. F. and Williams P. M. (1965) Concentration of bacteria from seawater by bubble scavenging. *ICES J. Marine Sci.*, *30*, 28–33.
- Castillo-Rogez J. C., Johnson T. V., Thomas P. C., Choukroun M., Matson D. L., and Lunine J. I. (2012) Geophysical evolution of Saturn's satellite Phoebe, a large planetesimal in the outer solar system. *Icarus*, *219*, 86–109, DOI: 10.1016/j.icarus.2012.02.002.
- Charnoz S., Crida A., Castillo-Rogez J. C., Lainey V., Dones L., Karatekin Ö., Tobie G., Mathis S., Le Poncin-Lafitte G., and Salmon J. J. (2011) Accretion of Saturn's mid-sized moons during the viscous spreading of young massive rings: Solving the paradox of silicate-poor rings versus silicate-rich moons. *Icarus*, *216*, 535–550, DOI: 10.1016/j.icarus.2011.09.017.
- Choblet G., Tobie G., Sotin C., Běhouňková M., Čadek O., Postberg F., and Souček O. (2017) Powering prolonged hydrothermal activity inside Enceladus. *Nature Astron.*, *1*, 841–847, DOI: 1038/s41550-017-0289-8.
- Chung D. H. (1971) Pressure coefficients of elastic constants for porous materials: Correction for porosity and discussion on literature data. *Earth Planet. Sci. Lett.*, *10*(3), 316–324.
- Consolmagno G. J. and Britt D. T. (1998) The density and porosity of meteorites from the Vatican collection. *Meteoritics & Planet. Sci.*, *33*(6), 1231–1241, DOI: 10.1111/j.1945-5100.1998.tb01308.x.
- Cowie G. L., Hedges J. I., Prahf F. G., and de Lange G. J. (1995) Elemental and major biochemical changes across an oxidation front in a relict turbidite: An oxygen effect. *Geochim. Cosmochim. Acta*, *59*, 33–46, DOI: 10.1016/0016-7037(94)00329-K.
- Coyette A., Baland R.-M., and Van Hoolst T. (2018) Variations in rotation rate and polar motion of a non-hydrostatic Titan. *Icarus*, *307*, 83–105, DOI: 10.1016/j.icarus.2018.02.003.
- Creamer J. S., Mora M. F., and Willis P. A. (2017) Enhanced resolution of chiral amino acids with capillary electrophoresis for biosignature detection in extraterrestrial samples. *Anal. Chem.*, *89*(2), 1329–1337.
- Crida A. and Charnoz S. (2012) Formation of regular satellites from ancient massive rings in the solar system. *Science*, *338*, 1196–1199, DOI: 10.1126/science.1226477.
- Crida A., Charnoz S., Hsu H.-W., and Dones L. (2019) Are Saturn's rings really young? *Nature Astron.*, *3*, 967–970.
- Cronin J. and Pizzarello S. (1983) Amino acids in meteorites. *Adv. Space Res.*, *3*(9), 5–18.
- Crow-Willard E. N. and Pappalardo R. T. (2015) Structural mapping of Enceladus and implications for formation of tectonized regions. *J. Geophys. Res.—Planets*, *120*, 928–950, DOI: 10.1002/2015JE004818.
- Cuk M., Dones L., and Nesvorný D. (2016) Dynamical evidence for a late formation of Saturn's moons. *Astrophys. J.*, *820*, 97, DOI: 10.3847/0004-637X/820/2/97.
- Davila A. F. and McKay C. P. (2014) Chance and necessity in biochemistry: Implications for the search for extraterrestrial biomarkers in Earth-life environments. *Astrobiology*, *14*, 534–540.
- Deamer D. W. and Damer B. (2017) Hydrothermal conditions and the origin of cellular life. *Astrobiology*, *17*, 834–839.
- Deamer D. W. and Georgiou C. D. (2015) Hydrothermal conditions and the origin of cellular life. *Astrobiology*, *15*, 1091–1095.
- Desch S. J., Kalyaan A., and Alexander C. M. O'D. (2018) The effect of Jupiter's formation on the distribution of refractory elements and inclusions in meteorites. *Astrophys. J. Suppl. Ser.*, *238*, 11.
- Des Marais D. J., Nuth J. A., Allamandola L. J., Boss A. P., Farmer J. D., Hoehler T. M., Jakosky B. M., Meadows V. S., Pohorille A., Runnegar B., and Spormann A. M. (2008) The NASA Astrobiology Roadmap. *Astrobiology*, *8*, 715–730.
- Dhingra D., Hedman M. M., Clark R. N., and Nicholson P. D. (2017) Spatially resolved near infrared observations of Enceladus' tiger stripe eruptions from Cassini VIMS. *Icarus*, *292*, 1–12.
- Dikarev V. V. (1999) Dynamics of particles in Saturn's E ring: Effects of charge variations and the plasma drag force. *Astron. Astrophys.*, *346*, 1011–1019.
- Dodd M. S., Papineau D., Grenne T., Slack J. F., Rittner M., Pirajno F., O'Neil J., and Little C. T. S. (2017) Evidence for early life in Earth's oldest hydrothermal vent precipitates. *Nature*, *543*, 60–64.
- Dong Y., Hill T. W., and Ye S.-Y. (2015) Characteristics of ice grains in the Enceladus plume from Cassini observations. *J. Geophys. Res.—Space Physics*, *120*, 915–937, DOI: 10.1002/2014JA020288.
- Dorn E. D., Nealon K. H., and Adami C. (2011) Monomer abundance distribution patterns as a universal biosignature: Examples from terrestrial and digital life. *J. Molec. Evol.*, *72*, 283–295.
- Dougherty M. K., Khurana K. K., Neubauer F. M., Russell C. T., Saur J., Leisner J. S., and Burton N. E. (2006) Identification of a dynamic atmosphere at Enceladus with the Cassini magnetometer. *Science*, *311*, 1406–1409, DOI: 10.1126/science.1120985.
- Drake F. (2003) The Drake equation revisited. *Astrobiology Magazine*, retrieved March 30, 2018, available online at <https://www.astrobio.net/alien-life/the-drake-equation-revisited-part-i>.
- Dunham E., Desch S. J., and Probst L. (2019) Haumea's shape, composition, and internal structure. *Astrophys. J.*, *877*, 41.
- Durham W. B., Kirby S. H., and Stern L. A. (1992) Effects of dispersed particulates on the rheology of water ice at planetary conditions. *J. Geophys. Res.*, *97*(E12), 20883–20897, DOI: 10.1029/92JE02326.
- Durham W. B., Prieto-Ballesteros O., Goldsby D. L., and Kargel J. S. (2010) Rheological and thermal properties of icy materials. *Space*

- Sci. Rev.*, 153, 273–298, DOI: 10.1007/s11214-009-9619-1.
- Ermakov A. I., Fu R. R., Castillo-Rogez J. C., Raymond C. A., Park R. S., Preusker F., Russell C. T., Smith D. E., and Zuber M. T. (2017) Constraints on Ceres' internal structure and evolution from its shape and gravity measured by the Dawn spacecraft. *J. Geophys. Res.–Planets*, 122(11), 2267–2293, DOI: 10.1002/2017JE005302.
- Etioppe G. and Sherwood Lollar B. (2013) Abiotic methane on Earth. *Rev. Geophys.*, 51, 276–299.
- Europa Lander Mission Concept Team (2016) *Europa Lander Study 2016 Report: Europa Lander Mission*, JPL D-97667, available online at [https://solarsystem.nasa.gov/docs/Europa\\_Lander\\_SDT\\_Report\\_2016.pdf](https://solarsystem.nasa.gov/docs/Europa_Lander_SDT_Report_2016.pdf).
- Fagerbakke K. M., Helgal M., and Norland S. (1996) Contents of carbon, oxygen, nitrogen, sulfur and phosphorus in native aquatic and cultured bacteria. *Aquat. Microb. Ecol.*, 10, 15–27.
- Feibelman W. (1967) Concerning the “D” ring of Saturn. *Nature*, 214, 793–794, DOI: 10.1038/214793a0.
- Fitch C. A., Platzer G., Okon M., Garcia-Moreno B., and McIntosh L. P. (2015) Arginine: Its pKa value revisited. *Protein Sci.*, 24(5), 752–761.
- Fortsch D., Pabst K., and Gross-Hardt E. (2015) The product distribution in Fischer–Tropsch synthesis: An extension of the ASF model to describe common deviations. *Chem. Eng. Sci.*, 138, 333–346.
- Fuller J., Luan J., and Eliot Quataert E. (2016) Resonance locking as the source of rapid tidal migration in the Jupiter and Saturn moon systems. *Mon. Not. R. Astron. Soc.*, 458(4), 3867–3879, DOI: 10.1093/mnras/stw609.
- Gao P., Kopparla P., Zhang X., and Ingersoll A. P. (2016) Aggregate particles in the plumes of Enceladus. *Icarus*, 264, 227–238.
- Georgiou C. D. and Deamer D. W. (2014) Lipids as universal biomarkers of extraterrestrial life. *Astrobiology*, 14, 541–549.
- Glavin D. P., Callahan M. P., Dworkin J. P., and Elsila J. E. (2010) The effects of parent body processes on amino acids in carbonaceous chondrites. *Meteoritics & Planet. Sci.*, 45, 1948–1972.
- Gleeson D. F., Pappalardo R. T., Anderson M. S., Grasby S. E., Mielke R. E., Wright K. E., and Templeton A. S. (2012) Biosignature detection at an Arctic analog to Europa. *Astrobiology*, 12(2), 135–150.
- Glein C. R., Baross J. A., and Waite J. H. (2015) The pH of Enceladus' ocean. *Geochim. Cosmochim. Acta*, 162, 202–219.
- Glein C. R., Postberg F., and Vance S. D. (2018) The geochemistry of Enceladus: Composition and controls. In *Enceladus and the Icy Moons of Saturn* (P. M. Schenk et al., eds.), pp. 39–56. Univ. of Arizona, Tucson.
- Goguen J. D., Buratti B. J., Brown R. H., Clark R. N., Nicholson P. D., Hedman M. M., Howell R. R., Sotin C., Cruikshank D. P., Baines K. H., Lawrence K. J., Spencer J. R., and Blackburn D. G. (2013) The temperature and width of an active fissure on Enceladus measured with Cassini VIMS during the 14 April 2012 south pole flyover. *Icarus*, 226(1), 1128–1137, DOI: 10.1016/j.icarus.2013.07.012.
- Haff P., Eviatar A., and Siscoe G. (1983) Ring and plasma: The enigmae of Enceladus. *Icarus*, 56(3), 426–438.
- Hansen C. J., Hendrix A., Esposito L., Colwell J., Shemansky D., Pryor W., Stewart I., and West R. (2005) Cassini Ultra Violet Imaging Spectrograph (UVIS) observations of Enceladus' plume. *Eos Trans. AGU*, 86(52), Fall Meet. Suppl., Abstract P21F-04.
- Hansen C. J., Esposito L., Stewart A. I. F., Colwell J., Hendrix A. P., Shemansky W. D., and West R. (2006) Enceladus' water vapor plume. *Science*, 311, 1422–1425, DOI: 10.1126/science.1121254.
- Hansen C., Esposito L., Stewart A., et al. (2008) Water vapour jets inside the plume of gas leaving Enceladus. *Nature*, 456, 477–479, DOI: 10.1038/nature07542.
- Hansen C. J. et al. (2011) The composition and structure of the Enceladus plume. *Geophys. Res. Lett.*, 38, L11202, DOI: 10.1029/2011GL047415.
- Hansen C. J., Esposito L. W., Aye K.-M., Colwell J. E., Hendrix A. R., Portyankina G., and Shemansky D. (2017) Investigation of diurnal variability of water vapor in Enceladus' plume by the Cassini ultraviolet imaging spectrograph. *Geophys. Res. Lett.*, 44, 672–677, DOI: 10.1002/2016GL071853.
- Hedman M. M., Nicholson P. D., Showalter M. R., Brown R. H., Buratti B. J., and Clark R. N. (2009) Spectral observations of the Enceladus plume with Cassini-VIMS. *Astrophys. J.*, 693, 1749–1762, DOI: 10.1088/0004-637X/693/2/1749.
- Hedman M., Gomsmeier C., Nicholson P., et al. (2013) An observed correlation between plume activity and tidal stresses on Enceladus. *Nature*, 500, 182–184, DOI: 10.1038/nature12371.
- Hedman M. M., Dhingra D., Nicholson P. D., Hansen C. J., Portyankina G., Ye S., and Dong Y. (2018) Spatial variations in the dust-to-gas ratio of Enceladus' plume. *Icarus*, 305, 123–138, DOI: 10.1016/j.icarus.2018.01.006.
- Hemingway D. J. and Mittal T. (2019) Enceladus' ice shell structure as a window on internal heat production. *Icarus*, 332, 111–131.
- Hemingway D. J., Rudolph M. L., and Manga M. (2020) Cascading parallel fractures on Enceladus. *ArXiv e-prints*, arXiv:1911.02730v1.
- Henning W. G. and Hurford T. (2014) Tidal heating in multilayered terrestrial exoplanets. *Astrophys. J.*, 789, 30.
- Higgs P. G. and Pudritz R. E. (2009) A thermodynamic basis for prebiotic amino acid synthesis and the nature of the first genetic code. *Astrobiology*, 9, 483–490.
- Hoehler T. M. (2004) Biological energy requirements as quantitative boundary conditions for life in the subsurface. *Geobiology*, 2, 205–215.
- Hoehler T. M. and Jørgensen B. B. (2013) Microbial life under extreme energy limitation. *Nature Rev. Microbiol.*, 11, 83–94.
- Hoehler T. M., Alperin M. J., Albert D. B., and Martens C. S. (2001) Apparent minimum free energy requirements for methanogenic Archaea and sulfate-reducing bacteria in an anoxic marine sediment. *FEMS Microbiol. Ecol.*, 38, 33–41.
- Holland G., Sherwood Lollar B., Li L., Lacrampe-Couloume G., Slater G. F., and Ballentine C. (2013) Deep fracture fluids isolated in the crust since the Precambrian era. *Nature*, 497(7449), 357–360, DOI: 10.1038/nature12127.
- Horányi M., Juhász A., and Morfill G. E. (2008) Large-scale structure of Saturn's E ring. *Geophys. Res. Lett.*, 35, L04203.
- Howell S. M. and Pappalardo R. T. (2019) Can Earth-like plate tectonics occur in ocean world ice shells? *Icarus*, 322, 69–79.
- Howett C. J. A., Spencer J. R., Pearl J., and Segura M. (2010) Thermal inertia and bolometric Bond albedo values for Mimas, Enceladus, Tethys, Dione, Rhea and Iapetus as derived from Cassini/CIRS measurements. *Icarus*, 206(2), 573–593.
- Howett C. J. A., Spencer J. R., Pearl J., and Segura M. (2011) High heat flow from Enceladus' south polar region measured using 10–600 cm<sup>-1</sup> Cassini/CIRS data. *J. Geophys. Res.–Planets*, 116(E3), E03003, DOI: 10.1029/2010JE003718.
- Hsu H. W., Postberg F., Sekine Y., Shibuya T., Kempf S., Horanyi M., Juhász A., Altobelli N., Suzuki K., Masaki Y., Kuwatani T., Tachibana S., Sirono S. I., Moragas-Klostermeyer G., and Srama R. (2015) Ongoing hydrothermal activities within Enceladus. *Nature*, 519, 207–210.
- Hsu H.-W., Schmidt J., Kempf S., Postberg F., Moragas-Klostermeyer G., Seiss M., Hoffmann H., Burton M., Ye S.-Y., Kurth W. S., Horanyi M., Khawaja N., Spahn F., Schirdehahn D., O'Donoghue J., Moore L., Cuzzi J., Jones G. H., and Srama R. (2018) *In situ* collection of dust grains falling from Saturn's rings into its atmosphere. *Science*, 362(6410), eaat3185.
- Hurley D. M., Perry M. E., and Waite J. H. (2015) Modeling insights into the locations of density enhancements from the Enceladus water vapor jets. *J. Geophys. Res.–Planets*, 120, 1763–1773, DOI: 10.1002/2015JE004872.
- Iess L., Stevenson D. J., Parisi M., Hemingway D., Jacobson R. A., Lunine J. I., Nimmo F., Armstrong J. W., Asmar S. W., Ducci M., and Tortora P. (2014) The gravity field and interior structure of Enceladus. *Science*, 344(6179), 78–80, DOI: 10.1126/science.1250551.
- Iess L., Militzer B., Kaspi Y., Nicholson P., Durante D., Racioppa P., Anabtawi A., Galanti E., Hubbard W., Mariani M. J., Tortora P., Wahl S., and Zannoni M. (2019) Measurement and implications of Saturn's gravity field and ring mass. *Science*, 364(6445), eaat2965, DOI: 10.1126/science.aat2965.
- Ingersoll A. P. and Ewald S. P. (2017) Decadal timescale variability of the Enceladus plumes inferred from Cassini images. *Icarus*, 282, 260–275, DOI: 10.1016/j.icarus.2016.09.018.
- Jaramillo-Botero A., An Q., Cheng M.-J., Goddard W., Beegle L., and Hodyss R. (2012) Hypervelocity impact effect of molecules from Enceladus' plume and Titan's upper atmosphere on NASA's Cassini Spectrometer from reactive dynamics simulation. *Phys. Rev. Lett.*, 109, 213201.
- Jia X., Kivelson M. G., Khurana K. K., and Kurth W. S. (2018)

- Evidence of a plume on Europa from Galileo magnetic and plasma wave signatures. *Nature Astron.*, 2, 459–464.
- Johansen A. and Lambrechts M. (2017) Forming planets via pebble accretion. *Annu. Rev. Astron. Astrophys.*, 45, 359–387.
- Johnson J. W., Oelkers E. H., and Helgeson H. C. (1992) SUPCRT92: A software package for calculating the standard molal thermodynamic properties of minerals, gases, aqueous species, and reactions from 1 to 5000 bar and 0° to 1000°C. *Computers Geosci.*, 18(7), 899–947, DOI: 10.1016/0098-3004(92)90029-Q.
- Jones G. H., Arridge C. S., Coates A. J., Lewis G. R., Kanani S., Wellbrock A., Young D. T., Cray F. J., Tokar R. L., Wilson R. J., Hill T. W., Johnson R. E., Mitchell D. G., Schmidt J., Kempf S., Beckmann U., Russell C. T., Jia Y. D., Dougherty M. K., Waite J. H., and Magee B. A. (2009) Fine jet structure of electrically charged grains in Enceladus' plume. *Geophys. Res. Lett.*, 36, L16204, DOI: 10.1029/2009GL038284.
- Jurac S., Johnson R. E., and Richardson J. D. (2001) Saturn's E ring and production of the neutral torus. *Icarus*, 149, 384–396.
- Kelley D. S., Karson J. A., Früh-Green G. L., Yoerger D. R., Shank T. M., Butterfield D. A., Hayes J. M., Schrenk M. O., Olson E. J., Proskurowski G., Jakuba M., Bradley A., Larson B., Ludwig K., Glickson D., Buckman K., Bradley A. S., Brazelton W. J., Roe K., Elend M. J., Delacour A., Bernasconi S. M., Lilley M. D., Baross J. A., Summons R. E., and Sylva S. P. (2005) A serpentinite-hosted ecosystem: The Lost City hydrothermal field. *Science*, 307(5714), 1428–1434.
- Kempf S., Beckmann U., Moragas-Klostermeyer G., Postberg F., Srama R., Economou T., Schmidt J., Spahn F., and Grun E. (2008) The E ring in the vicinity of Enceladus I. Spatial distribution and properties of the ring particles. *Icarus*, 193, 420–437, DOI: 10.1016/j.icarus.2007.06.027.
- Kempf S., Beckmann U., and Schmidt J. (2010) How the Enceladus dust plume feeds Saturn's E ring. *Icarus*, 206, 446–457, DOI: 10.1016/j.icarus.2009.09.016.
- Khawaja N., Postberg F., Hillier J., Klenner F., Kempf S., Nolle L., Reviol R., Zou Z., and Srama R. (2019) Low mass nitrogen-, oxygen-bearing and aromatic compounds in Enceladean ice grains. *Mon. Not. R. Astron. Soc.*, 489(4), 5231–5243.
- Kirchoff M. R. and Schenk P. (2009) Crater modification and geologic activity in Enceladus' heavily cratered plains: Evidence from the impact crater distribution. *Icarus*, 202(2), 656–668.
- Kirchoff M. R., Bierhaus E. B., Dones L., Robbins S. J., Singer K. N., Wagner R. J., and Zahnle K. J. (2018) Cratering histories in the saturnian system. In *Enceladus and the Icy Moons of Saturn* (P. M. Schenk et al., eds.), pp. 267–284. Univ. of Arizona, Tucson.
- Kirk R. L., Soderblom L. A., Brown R. H., Kieffer S. W., and Kargel J. S. (1995) Triton's plumes: Discovery, characteristics, and models. In *Neptune and Triton* (D. P. Cruikshank, ed.), pp. 949–989. Univ. of Arizona, Tucson.
- Kite E. S. and Rubin A. M. (2016) Sustained eruptions on Enceladus explained by turbulent dissipation in tiger stripes. *Proc. Natl. Acad. Sci. USA*, 113, 3972–3975.
- Klein H. P. (1978) The Viking biological experiments on Mars. *Icarus*, 34(3), 666–674, DOI: 10.1016/0019-1035(78)90053-2.
- Klenner F., Postberg F., Hillier J., Khawaja N., Reviol R., Stolz F., Cable M. L., Abel B., and Nölle L. (2020) Analog experiments for the identification of trace biosignatures in ice grains from extraterrestrial ocean worlds. *Astrobiology*, 20, 179–189.
- Klimczak C., Byrne P. K., Regensburger P. V., Bohnenstiehl D. R., Hauck S. A., Dombard A. J., Hemingway D. J., Vance S. D., Melwani Daswani M., and Elder C. M. (2019) Strong ocean floors with Europa, Titan, and Ganymede limit geological activity there, Enceladus less so. *Lunar Planet. Sci. L*, Abstract #2132. Lunar and Planetary Institute, Houston.
- Lainey V., Jacobson R. A., Tajeddine R., Cooper N. J., Murray C., Robert V., Tobie G., Guillot T., Mathis S., Remus F., Desmars J., Arlot J.-E., De Cuyper J.-P., Dehant V., Pascu D., Thuillot W., LePoncin-Lafitte C., and Zahn J.-P. (2017) New constraints on Saturn's interior from Cassini astrometric data. *Icarus*, 281, 286–296, DOI: 10.1016/j.icarus.2016.07.014.
- Lane N. and Martin W. F. (2012) The origin of membrane bioenergetics. *Cell*, 151, 1406–1416.
- Li Y. and Breaker R. (1999) Kinetics of RNA degradation by specific base catalysis of transesterification involving the 2'-hydroxyl group. *J. Am. Chem. Soc.*, 121, 5364–5372.
- Lingham M. and Loeb A. (2018) Is extraterrestrial life suppressed on subsurface ocean worlds due to the paucity of bioessential elements? *Astron. J.*, 156, 151, DOI: 10.3847/1538-3881/aada02.
- Maffei T., Sommariva S., Ranzi E., and Faravelli T. (2012) A predictive kinetic model of sulfur release from coal. *Fuel*, 91(1), 213–223, DOI: 10.1016/j.fuel.2011.08.017.
- Maffei T., Frassoldati A., Cuoci A., Ranzi E., and Faravelli T. (2013) Predictive one step kinetic model of coal pyrolysis for CFD applications. *Proc. Comb. Inst.*, 34(2), 2401–2410, DOI: 10.1016/j.proci.2012.08.006.
- Magee B. H. and Waite J. H. (2017) Neutral gas composition of Enceladus' plume — Model parameter insights from Cassini-INMS. *Lunar Planet. Sci. XLVIII*, Abstract #2974. Lunar and Planetary Institute, Houston.
- Marchetto C. A. (1983) The Voyager 2 scan platform anomaly. *Guidance and Control, Proceedings of the Annual Rocky Mountain Conference*, 219–243. Keystone, Colorado, Feb. 5–9, AAS paper 83-046, available online at <https://ntrs.nasa.gov/search.jsp?R=19830062955>.
- Mason B. (1979) Chapter B, Cosmochemistry, Part 1. Meteorites. In *Data of Geochemistry, 6th edition* (M. Fleischer, ed.), U.S. Geological Survey Professional Paper 440-B-1.
- Mason D. L., Castillo-Rogez J. C., Davies A. G., and Johnson T. V. (2012) Enceladus: A hypothesis for bringing both heat and chemicals to the surface. *Icarus*, 221(1), 53–62.
- McCarthy C. and Cooper R. F. (2016) Tidal dissipation in creeping ice and the thermal evolution of Europa. *Earth Planet. Sci. Lett.*, 443, 185–194, DOI: 10.1016/j.epsl.2016.03.006.
- McCollom T. M. (2016) Abiotic methane formation during experimental serpentinization of olivine. *Proc. Natl. Acad. Sci.*, 113(49), 13965–13970.
- McCollom T. M. and Amend J. P. (2005) A thermodynamic assessment of energy requirements for biomass synthesis by chemolithoautotrophic micro-organisms in oxic and anoxic environments. *Geobiology*, 3, 135–144.
- McCollom T. M. and Bach W. (2009) Thermodynamic constraints on hydrogen generation during serpentinization of ultramafic rocks. *Geochim. Cosmochim. Acta*, 73, 856–875.
- McCollom T. M. and Seewald J. S. (2001) A reassessment of the potential for reduction of dissolved CO<sub>2</sub> to hydrocarbons during serpentinization of olivine. *Geochim. Cosmochim. Acta*, 65(21), 3769–3778, DOI: 10.1016/S0016-7037(01)00655-X.
- McCollom T. M. and Seewald J. S. (2007) Abiotic synthesis of organic compounds in deep-sea hydrothermal environments. *Chem. Rev.*, 107, 382–401, DOI: 10.1021/cr0503660.
- McDermott J. M., Seewald J. S., German C. R., and Sylva S. P. (2015) Pathways for abiotic synthesis at submarine hydrothermal fluids. *Proc. Natl. Acad. Sci.*, 112(25), 7668–7672.
- McDonald A. H. and Fyfe W. S. (1985) Rate of serpentinization in seafloor environments. *Tectonophysics*, 116(1–2), 123–135, DOI: 10.1016/0040-1951(85)90225-2.
- McKay C. P. (2004) What is life — and how do we search for it in other worlds? *PLOS Biology*, 2(9), e302, DOI: 10.1371/journal.pbio.0020302.
- McKay C. P., Anbar A. D., Porco C., and Tsou P. (2014) Follow the plume: The habitability of Enceladus. *Astrobiology*, 14(4), 352–355, DOI: 10.1089/ast.2014.1158.
- McKay D. S., Gibson E. K., Thomas-Keptra K. L., and Vali H. (1996) Search for past life on Mars: Possible relic biogenic activity in martian meteorite ALH84001. *Science*, 273(5277), 924–930, DOI: 10.1126/science.273.5277.924.
- McKinnon W. B. (2015) Effect of Enceladus's rapid synchronous spin on interpretation of Cassini gravity. *Geophys. Res. Lett.*, 42(7), 2137–2143.
- McKinnon W. B. and Zolensky M. E. (2003) Sulfate content of Europa's ocean and shell: Evolutionary considerations and some geological and astrobiological implications. *Astrobiology*, 3(4), 879–897, DOI: 10.1089/15311070322736150.
- McKinnon W. B., Prialnik D., Stern S. A., and Coradini A. (2008) Structure and evolution of Kuiper belt objects and dwarf planets. In *The Solar System Beyond Neptune* (M. A. Barucci et al., eds.), pp. 213–241. Univ. of Arizona, Tucson.
- Meier P., Krieger H., Motschmann U., Schmidt J., Spahn F., Hill T. W., Dong Y., and Jones G. H. (2014) A model of the spatial and size distribution of Enceladus' dust plume. *Planet. Space Sci.*, 104, 216–233, DOI: 10.1016/j.pss.2014.09.016.



- Menez B., Pisapia C., Andreani M., Jamme F., Vanbellinghen Q. P., Brunelle A., Richard L., Dumas P., and Refregiers M. (2018) Abiotic synthesis of amino acids in the recesses of the oceanic lithosphere. *Nature*, 564, 59–63.
- Meyer J. and Wisdom J. (2007) Tidal heating in Enceladus. *Icarus*, 188, 535–539.
- Mitchell C. J., Porco C. C., and Weiss J. W. (2015) Tracking the geysers of Enceladus into Saturn's E ring. *Astron. J.*, 149, 156, DOI: 10.1088/0004-6256/149/5/156.
- Mitchell K. A., Ono M., Parcheta C., and Iacoponi S. (2017) Dynamic pressure at Enceladus' vents and implications for vent and conduit in-situ studies. *Lunar Planet Sci. XLVIII*, Abstract #2801. Lunar and Planetary Institute, Houston.
- Mitchell K. L. (2014) Cryovolcanic conduit evolution and eruption on icy satellites. Abstract P52A-02 presented at 2014 Fall Meeting, AGU, San Francisco, California, 15–19 December.
- Moldowan J. M., Seifert W. K., and Gallegos E. J. (1985) Relationship between petroleum composition and depositional environment of petroleum source rocks. *Am. Assoc. Petrol. Geol. Bull.*, 69, 1255–1268.
- Mosqueira I. and Estrada P. R. (2003a) Formation of the regular satellites of giant planets in an extended gaseous nebula I: Subnebula model and accretion of satellites. *Icarus*, 163, 198–231.
- Mosqueira I. and Estrada P. R. (2003b) Formation of the regular satellites of giant planets in an extended gaseous nebula II: Satellite migration and survival. *Icarus*, 163, 232–255.
- Mottl M. J. and Holland H. D. (1978) Chemical exchange during hydrothermal alteration of basalt by seawater — I. Experimental results for major and minor components of seawater. *Geochim. Cosmochim. Acta*, 42(8), 1103–1115, DOI: 10.1016/0016-7037(78)90107-2.
- Mouis O. and Alibert Y. (2006) Modeling the jovian subnebula II. Composition of regular satellite ices. *Astron. Astrophys.*, 448, 771–778.
- Mouis O., Chassefière E., Holm N. G., Bouquet A., Waite J. H., Geppert W. D., Picaut S., Aikawa Y., Ali-Dib M., Charlou J.-L., and Rousselot P. (2015) Methane clathrates in the solar system. *Astrobiology*, 15(4), 308–326, DOI: 10.1089/ast.2014.1189.
- Mumma M. J. and Charnley S. B. (2011) The chemical composition of comets — emerging taxonomies and natal heritage. *Annu. Rev. Astron. Astrophys.*, 49(1), 471–524, DOI: 10.1146/annurev-astro-081309-130811.
- Nakajima M. and Ingersoll A. P. (2016) Controlled boiling on Enceladus. I. Model of the vapor-driven jets. *Icarus*, 272, 309–318.
- National Research Council (2012) *Assessment of Planetary Protection Requirements for Spacecraft Missions to Icy Solar System Bodies*. National Academies, Washington, DC, DOI: 10.17226/13401.
- Neveu M. and Rhoden A. R. (2019) Evolution of Saturn's mid-sized moons. *Nature Astron.*, 3, 543–552.
- Neveu M., Glein C. R., Anbar A. D., McKay C. P., Desch S. J., Castillo-Rogez J. C., and Tsou P. (2014) Enceladus' fully cracked core: Implications for habitability. *Workshop on the Habitability of Icy Worlds*, Abstract #4028. Lunar and Planetary Institute, Houston.
- Neveu M., Desch S. J., and Castillo-Rogez J. C. (2015) Core cracking and hydrothermal circulation can profoundly affect Ceres' geophysical evolution. *J. Geophys. Res.—Planets*, 120, 123–154, DOI: 10.1002/2014JE004714.
- Neveu M., Desch S. J., and Castillo-Rogez J. C. (2017) Aqueous geochemistry in icy world interiors: Equilibrium fluid, rock, and gas compositions, and fate of antifreezes and radionuclides. *Geochim. Cosmochim. Acta*, 212, 324–371, DOI: 10.1016/j.gca.2017.06.023.
- Neveu M., Hays L. E., Voytek M. A., New M. H., and Schulte M. D. (2018) The Ladder of Life Detection. *Astrobiology*, 18, 1375–1402.
- Nimmo F., Porco C. and Mitchell C. (2014) Tidally modulated eruptions on Enceladus: Cassini ISS observations and models. *Astron. J.*, 148, 46.
- Nimmo F., Barr A. C., Běhouňková M., and McKinnon W. B. (2018) The thermal and orbital evolution of Enceladus: Observational constraints and models. In *Enceladus and the Icy Moons of Saturn* (P. M. Schenk et al., eds.), pp. 79–94. Univ. of Arizona, Tucson.
- Oelkers E. H., Bénézet P., and Pokrovski G. S. (2009) Thermodynamic databases for water-rock interaction. *Rev. Min. Geochem.*, 70(1), 1–46, DOI: 10.2138/rmg.2009.70.1.
- Oh M. S., Crawford R. W., Foster K. G., and Alcaraz A. (1988) Ammonia evolution from western and eastern oil shales. *Division of Petroleum Chemistry, Preprints (USA)*, 34(1), 94–102, American Chemical Society.
- Ohmoto H. and Lasaga A. C. (1982) Kinetics of reactions between aqueous sulfates and sulfides in hydrothermal systems. *Geochim. Cosmochim. Acta*, 46(10), 1727–1745, DOI: 10.1016/0016-7037(82)90113-2.
- O'Neill C. and Nimmo F. (2010) The role of episodic overturn in generating the surface geology and heat flow on Enceladus. *Nature Geosci.*, 3, 88–91, DOI: 10.1038/ngeo731.
- Palandri J. L. and Kharaka Y. K. (2004) *A Compilation of Rate Parameters of Water-Mineral Interaction Kinetics for Application to Geochemical Modeling*. U.S. Geological Survey Open File Report 2004-1068, 71 pp., available online at <http://www.dtic.mil/dtic/tr/fulltext/u2/a440035.pdf>.
- Parkinson C. D., Liang M.-C., Yung Y. L., and Kirschvink J. L. (2008) Habitability of Enceladus: Planetary conditions for life. *Orig. Life Evol. Biosph.*, 38(4), 355–369, DOI: 10.1007/s11084-008-9135-4.
- Parnell J., Cullen D., Sims M. R., Bowden S., Cockell C. S., Court R., Ehrenfreund P., Gaubert F., Grant W., and Parro V. (2007) Searching for life on Mars: Selection of molecular targets for ESA's aurora ExoMars mission. *Astrobiology*, 7, 578–604.
- Patthoff D. and Kattenhorn S. (2011) A fracture history on Enceladus provides evidence for a global ocean. *Geophys. Res. Lett.*, 38, L18201.
- Patthoff D., Kattenhorn S. A., and Cooper C. M. (2019) Implications of nonsynchronous rotation on the deformational history and ice shell properties in the south polar terrain of Enceladus. *Icarus*, 321, 445–457.
- Perry M. E., Teolis B. D., Hurley D. M., Magee B. A., Waite J. H., Brockwell T. G., Perryman R. S., and McNutt R. L. (2015) Cassini INMS measurements of Enceladus plume density. *Icarus*, 257, 139–162, DOI: 10.1016/j.icarus.2015.04.037.
- Phillips O. M. (1991) *Flow and Reactions in Permeable Rocks*. Cambridge Univ., Cambridge.
- Poch O., Joachim F., Isabel R., Antoine P., Bernhard J., and Nicolas T. (2017) Remote sensing of potential biosignatures from rocky, liquid or icy (exo)planetary surfaces. *Astrobiology*, 17(3), 231–252.
- Pokrovsky O. S. and Schott J. (1999) Processes at the magnesium-bearing carbonates/solution interface. II. Kinetics and mechanism of magnesite dissolution. *Geochim. Cosmochim. Acta*, 63(6), 881–897, DOI: 10.1016/S0016-7037(99)00013-7.
- Porco C. C., Helfenstein P., Thomas P. C., Ingersoll A. P., Wisdom J., West R., Neukum G., Denk T., Wagner R., Roatsch T., Kieffer S., Turtle E., McEwen A., Johnson T. V., Rathbun J., Veverka J., Wilson D., Perry J., Spitale J., Brahic A., Burns J. A., Del Genio A. D., Dones L., Murray C. D., and Squyres S. (2006) Cassini observes the active south pole of Enceladus. *Science*, 311(5766), 1393–1401, DOI: 10.1126/science.1123013.
- Porco C. C., DiNino D., and Nimmo F. (2014) How the geysers, tidal stresses, and thermal emission across the south polar terrain of Enceladus are related. *Astron. J.*, 148(3), 24 pp.
- Porco C. C., Dones L., and Mitchell C. (2017) Could it be snowing microbes on Enceladus? Assessing conditions in its plume and implications for future missions. *Astrobiology*, 17(9), 876–901.
- Porco C., Mitchell C. J., Nimmo F., and Tiscareno M. S. (2018) Multiple long-period variations in the plume of Enceladus offer insights into eruption mechanism. Abstract P34F-3819 presented at 2018 Fall Meeting, AGU, Washington, DC, 10–14 December.
- Postberg F., Kempf S., Hillier J. K., Srama R., Green S. F., McBride N., and Grün E. (2008) The E-ring in the vicinity of Enceladus II. Probing the moon's interior — the composition of E-ring particles. *Icarus*, 193, 438–454, DOI: 10.1016/j.icarus.2007.09.001.
- Postberg F., Kempf S., Schmidt J., Brilliantov N., Beinsen A., Abel B., Buck Y., and Srama R. (2009) Sodium salts in E ring ice grains from an ocean below the surface of Enceladus. *Nature*, 459, 1098–1101, DOI: 10.1038/nature08046.
- Postberg F., Schmidt J., Hillier J., Kempf S., and Srama R. (2011) A salt-water reservoir as the source of a compositionally stratified plume on Enceladus. *Nature*, 474(7353), 620–622, DOI: 10.1038/nature10175.
- Postberg F., Khawaja N., Abel B., Choblet G., Glein C. R., Gudipati M. S., Henderson B. L., Hsu H.-W., Kempf S., Klenner F., Moragas-Klostermeyer G., Magee B., Nolle L., Perry M., Reviel R., Schmidt J., Srama R., Stolz F., Tobie G., Trierloff M., and Waite J. H. (2018) Macromolecular organic compounds from the depths of Enceladus.



- Nature*, 558, 564–568.
- Renaud J. P. and Henning W. G. (2018) Increased tidal dissipation using advanced rheological models: Implications for Io and tidally active exoplanets. *Astrophys. J.*, 857(2), 98.
- Rivkin A. S., Asphaug E., and Bottke W. S. (2014) The case of the missing Ceres family. *Icarus*, 243, 429–439, DOI: 10.1016/j.icarus.2014.08.007.
- Roadcap G. S., Sanford R. A., Jin Q., Pardinás J. R., and Bethke C. M. (2006) Extremely alkaline (pH >12) ground water hosts diverse microbial community. *Groundwater*, 44(4), 511–517.
- Roberts J. H. (2015) The fluffy core of Enceladus. *Icarus*, 258, 54–66, DOI: 10.1016/j.icarus.2015.05.033.
- Roberts J. H. and Stickle A. M. (2017) Break the world's shell: An impact on Enceladus: Bringing the ocean to the surface. *Lunar Planet. Sci. XLVIII*, Abstract #1955. Lunar and Planetary Institute, Houston.
- Rodriguez M. M., Bill E., Brennessel W. W., and Holland P. L. (2011) N<sub>2</sub> reduction and hydrogenation to ammonia by a molecular iron-potassium complex. *Science*, 334(6057), 780–783, DOI: 10.1126/science.1211906.
- Rothschild L. and Mancinelli R. (2001) Life in extreme environments. *Nature*, 409, 1092–1101.
- Rubin M., Altwegg K., Balsiger H., Bar-Nun A., Berthelier J.-J., Bieler A., Bochsler P., Briois C., Calmonte U., Combi M., De Keyser J., Dhooghe F., Eberhardt P., Fiethé B., Fuselier S. A., Gasc S., Gombosi T. I., Hansen K. C., Hässig M., Jäckel A., Kopp E., Korth A., Le Roy L., Mall U., Marty B., Mousis O., Owen T., Rème H., Sémon T., Tzou C.-Y., Waite J. H., and Wurz P. (2015) Molecular nitrogen in Comet 67P/Churyumov-Gerasimenko indicates a low formation temperature. *Science*, aaa6100, DOI: 10.1126/science.aaa6100.
- Russell M. J., Barge L. M., Bhartia R., Bocanegra D., Bracher P. J., Branscomb E., Kidd R., McGlynn S., Meier D. H., Nitschke W., Shibuya T., Vance S., White L., and Kanik I. (2014) The drive to life on wet and icy worlds. *Astrobiology*, 14, 308–343.
- Russell M. J., Murray A. E., and Hand K. P. (2017) The possible emergence of life and differentiation of a shallow biosphere on irradiated icy worlds: The example of Europa. *Astrobiology*, 17(12), 1265–1273.
- Salmon J. J. and Canup R. M. (2017) Accretion of Saturn's inner mid-sized moons from a massive primordial ice ring. *Astrophys. J.*, 836, 109, DOI: 10.3847/1538-4357/836/1/109.
- Schenk P., Hamilton D. P., Johnson R. E., McKinnon W. B., Paranicas C., Schmidt J., and Showalter M. R. (2011) Plasma, plumes and rings: Saturn system dynamics as recorded in global color patterns on its midsize icy satellites. *Icarus*, 211, 740–757.
- Schink B. (1997) Energetics of syntrophic cooperation in methanogenic degradation. *Microbiol. Molec. Biol. Rev.*, 61, 262–280.
- Schmidt J., Brilliantov N., Spahn F., and Kempf S. (2008) Slow dust in Enceladus' plume from condensation and wall collisions in tiger stripe fractures. *Nature*, 451, 685–688, DOI: 10.1038/nature06491.
- Schrenk M. O., Kelley D. S., Bolton S. A., and Baross J. A. (2004) Low archaeal diversity linked to subseafloor geochemical processes at the Lost City Hydrothermal Field, Mid-Atlantic Ridge. *Environ. Microbiol.*, 6, 1086–1095.
- Schubert G., Anderson J. D., Travis B. J., and Palguta J. (2007) Enceladus: Present internal structure and differentiation by early and long-term radiogenic heating. *Icarus*, 188, 345–355, DOI: 10.1016/j.icarus.2006.12.012.
- Schubert G., Sohl F., and Hussmann H. (2009) Interior of Europa. In *Europa* (R. T. Pappalardo et al., eds.), pp. 353–367. Univ. of Arizona, Tucson.
- Schulte M. D. and Shock E. L. (2004) Coupled organic synthesis and mineral alteration on meteorite parent bodies. *Meteoritics & Planet. Sci.*, 39(9), 1577–1590, DOI: 10.1111/j.1945-5100.2004.tb00128.x.
- Seewald J. S. (2017) Detecting molecular hydrogen on Enceladus. *Science*, 356(6334), 132–133.
- Sekine Y., Shibuya T., Postberg F., Hsu H.-W., Suzuki K., Masaki Y., Kuwatani T., Mori M., Hong P. K., Yoshizaki M., Tachibana S., and Sirono S. (2015) High-temperature water-rock interactions and hydrothermal environments in the chondrite-like core of Enceladus. *Nature Commun.*, 6(8604), 1–8, DOI: 10.1038/ncomms9604.
- Seyfried W. E. and Mottl M. J. (1982) Hydrothermal alteration of basalt by seawater under seawater-dominated conditions. *Geochim. Cosmochim. Acta*, 46(6), 985–1002, DOI: 10.1016/0016-7037(82)90054-0.
- Shemansky D., Matheson P., Hall D., et al. (1993) Detection of the hydroxyl radical in the Saturn magnetosphere. *Nature*, 363, 329–331, DOI: 10.1038/363329a0.
- Sherwood B. (2016) Strategic map for exploring the ocean-world Enceladus. *Acta Astron.*, 126, 52–58.
- Sherwood Lollar B., Frapé S. K., Weise S. M., Fritz P., Macko S. A., and Welhan J. A. (1993) Abiogenic methanogenesis in crystalline rocks. *Geochim. Cosmochim. Acta*, 57(23), 5087–5097, DOI: 10.1016/0016-7037(93)90610-9.
- Sherwood-Lollar B., Westgate T. D., Ward J. A., Slater G. F., and Lacrampe-Couloume G. (2002) Abiogenic formation of alkanes in the Earth's crust as a minor source for global hydrocarbon reservoirs. *Nature*, 416(6880), 522–524, DOI: 10.1038/416522a.
- Shock E. L. and McKinnon W. B. (1993) Hydrothermal processing of cometary volatiles — applications to Triton. *Icarus*, 106(2), 464–477, DOI: 10.1006/icar.1993.1185.
- Sleep N. H., Meibom A., Fridriksson T., Coleman R. G., and Bird D. K. (2004) H<sub>2</sub>-rich fluids from serpentinization: Geochemical and biotic implications. *Proc. Natl. Acad. Sci. USA*, 101(35), 12818–12823, DOI: 10.1073/pnas.0405289101.
- Slonczewski L., Fujisawa M., Dopson M., and Krulwich T. A. (2009) Cytoplasmic pH measurement and homeostasis in *Bacteria* and *Archaea*. *Adv. Microb. Physiol.*, 55, 1–79.
- Smith H. T., Johnson R. E., Perry M. E., Mitchell D. G., McNutt R. L., and Young D. T. (2010) Enceladus plume variability and the neutral gas densities in Saturn's magnetosphere. *J. Geophys. Res.*, 115, A10252, DOI: 10.1029/2009JA015184.
- Southworth B. S., Kempf S., Spitale J., Srama R., Schmidt J., and Postberg F. (2017) Resolving the mass production and surface structure of the Enceladus dust plume. *Lunar Planet. Sci. XLVIII*, Abstract #2904. Lunar and Planetary Institute, Houston.
- Southworth B. S., Kempf S., and Spitale J. (2019) Surface deposition of the Enceladus plume and the zenith angle of emissions. *Icarus*, 319, 33–42.
- Spahn F., Schmidt J., Albers N., Hörning M., Makuch M., Seiss M., Kempf S., Srama R., Dikarev V., Helfert S., Moragas-Klostermeyer G., Krivov A. V., Sremčević M., Tuzzolino A. J., Economou T., and Grün E. (2006) Cassini dust measurements at Enceladus and implications for the origin of the E ring. *Science*, 311(5766), 1416–1418, DOI: 10.1126/science.1121375.
- Sparks W. B., Schmidt B. E., McGrath M. A., Hand K. P., Spencer J. R., Cracraft M., and Deustua S. E. (2017) Active cryovolcanism on Europa? *Astrophys. J. Lett.*, 839(2), L18.
- Spencer J. R. and Nimmo F. (2013) Enceladus: An active ice world in the Saturn system. *Annu. Rev. Earth Planet. Sci.*, 41, 693–717, DOI: 10.1146/annurev-earth-050212-124025.
- Spencer J. R., Pearl J. C., Segura M., Flasar F. M., Mamoutkine A., Romani P., Burratti B. J., Hendrix A. R., Spilker L. J., and Lopes R. M. C. (2006) Cassini encounters Enceladus: Background and the discovery of a south polar hot spot. *Science*, 311(5766), 1401–1405, DOI: 10.1126/science.1121661.
- Spitale J. N., Hurford T. A., Rhoden A. R., Berkson E. E., and Platts S. S. (2015) Curtain eruptions form Enceladus' south-polar terrain. *Nature*, 521, 57–60.
- Spitale J. N., Hurford T., and Rhoden A. R. (2017) Short-term variability in Enceladus' plume. *AAS/Division for Planetary Sciences Meeting Abstracts*, 49, 207.02.
- Steel E., Davila A., and McKay C. P. (2017) Abiotic and biotic formation of amino acids in the Enceladus ocean. *Astrobiology*, 17(9), 862–875.
- Stone E. C. and Miner E. D. (1981) Voyager 1 encounter with the saturnian system. *Science*, 212(4491), 159–163.
- Storrie-Lombardi M. C. and Sattler B. (2009) Laser-induced fluorescence emission (L.I.F.E.): In situ nondestructive detection of microbial life in the ice covers of Antarctic lakes. *Astrobiology*, 9(7), 659–672.
- Stryk T. (2017) Pre-discovery detection of the plumes of Enceladus. *Lunar Planet. Sci. XLVIII*, Abstract #1603. Lunar and Planetary Institute, Houston.
- Summons R. E., Albrecht P., McDonald G., and Moldowan J. M. (2008) Molecular biosignatures. *Space Sci. Rev.*, 135, 133–159.
- Taubner R. S., Schleper C., Firneis M. G., and Rittmann S. K. M. R. (2015) Assessing the ecophysiology of methanogens in the context of recent astrobiological and planetological studies. *Life*, 5, 1652–

- 1686.
- Taubner R. S., Pappenreiter P., Zwicker J., Smrzka D., Pruckner C., Kolar P., Bernacchi S., Seifert A. H., Krajete A., Bach W., Peckmann J., Paulik C., Firneis M. G., Schleper C., and Rittmann S. K. (2018) Biological methane productions under putative Enceladus-like conditions. *Nature Commun.*, 9, 748.
- Teolis B. D., Perry M. E., Magee B. A., Westlake J., and Waite J. H. (2010) Detection and measurement of ice grains and gas distribution in the Enceladus plume by Cassini's Ion Neutral Mass Spectrometer. *J. Geophys. Res.*, 115, A09222.
- Teolis B. D., Perry M. E., Hansen C. J., Waite J. H., Porco C. C., Spencer J. R., and Howett C. J. A. (2017) Enceladus plume structure and time variability: Comparison of Cassini observations. *Astrobiology*, 17(9), 926–940.
- Terrile R. J. and Cook A. F. (1981) Enceladus: Evolution and possible relationship to Saturn's E-ring. *Lunar Planet. Sci. XII, Suppl. A, Satellites of Saturn*, p. 10. LPI Contribution No. 428, Lunar and Planetary Institute, Houston.
- Thauer R. K., Kaster A. K., Seedorf H., Buckel W., and Hedderich R. (2008) Methanogenic archaea: Ecologically relevant differences in energy conservation. *Nature Rev. Microbiol.*, 6, 579–591.
- Thomas P. C., Tajeddine R., Tiscareno M. S., Burns J. A., Joseph J., Loredi T. J., Helfenstein P., and Porco C. (2016) Enceladus's measured physical libration requires a global subsurface ocean. *Icarus*, 264, 37–47, DOI: 10.1016/j.icarus.2015.08.037.
- Tian F., Stewart A. I. F., Toon O. B., Larsen K. W., and Esposito L. W. (2007) Monte Carlo simulations of the water vapor plumes on Enceladus. *Icarus*, 188(1), 154–161, DOI: 10.1016/j.icarus.2006.11.010.
- Tijhuis L., van Loosdrecht M. C. M., and Heijnen J. J. (1993) A thermodynamically based correlation for maintenance Gibbs energy requirements in aerobic and anaerobic chemotrophic growth. *Biotech. Bioeng.*, 42, 509–519.
- Tokar R. L., Johnson R. E., Hill T. W., Pontius D. H., Kurth W. S., Cray F. J., Young D. T., Thomsen M. F., Reisenfeld D. B., Coates A. J., Lewis G. R., Sittler E. C., and Gurnett D. A. (2006) The interaction of the atmosphere of Enceladus with Saturn's plasma. *Science*, 311, 1409–1412, DOI: 10.1126/science.1121061.
- Tortora P., Zannoni M., Hemingway D., Nimmo F., Jacobson R. A., Iess L., and Parisi M. (2016) Rhea gravity field and interior modeling from Cassini data analysis. *Icarus*, 264, 264–273, DOI: 10.1016/j.icarus.2015.09.022.
- Truong N., Monroe A. A., Glein C. R., Anbar A. D., and Lunine J. I. (2019) Decomposition of amino acids in water with application to in-situ measurements of Enceladus, Europa and other hydrothermally active icy ocean worlds. *Icarus*, 329, 140–147.
- Travis B. J. and Schubert G. (2015) Keeping Enceladus warm. *Icarus*, 250, 32–42, DOI: 10.1016/j.icarus.2014.11.017.
- Tsou P., Brownlee D. E., McKay C. P., Anbar A. D., Yano H., Altwegg K., Beegle L. W., Dissly R., Strange N. J., and Kanik I. (2012) LIFE: Life Investigation For Enceladus — A sample return mission concept in search for evidence of life. *Astrobiology*, 12, 730–742, DOI: 10.1089/ast.2011.0813.
- Tyburczy J. A., Duffy T. S., Ahrens T. J., and Lange M. A. (1991) Shock wave equation of state of serpentine to 150 GPa: Implications for the occurrence of water in the Earth's lower mantle. *J. Geophys. Res.—Solid Earth*, 96(B11), 18011–18027, DOI: 10.1029/91JB01573.
- Tyler R. (2014) Comparative estimates of the heat generated by ocean tides on icy satellites in the outer solar system. *Icarus*, 243, 358–385, DOI: 10.1016/j.icarus.2014.08.037.
- Vance S., Harnmeijer J., Kimura J., Hussmann H., deMartin B., and Brown J. M. (2007) Hydrothermal systems in small ocean planets. *Astrobiology*, 7(6), 987–1005, DOI: 10.1089/ast.2007.0075.
- Vance S. D., Hand K. P., and Pappalardo R. T. (2016) Geophysical controls of chemical disequilibria in Europa. *Geophys. Res. Lett.*, 43, 4871–4879.
- Verbiscer A., French R., Showalter M., and Helfenstein P. (2007) Enceladus: Cosmic graffiti artist caught in the act. *Science*, 315(5813), 815.
- Waite J. H., Combi M. R., Ip W.-H., Cravens T. E., McNutt R. L., Kasprzak W., Yelle R., Luhmann J., Niemann H., Gell D., Magee B., Fletcher G., Lunine J. I., and Tseng W.-L. (2006) Cassini ion and neutral mass spectrometer: Enceladus plume composition and structure. *Science*, 311(5766), 1419–1422, DOI: 10.1126/science.1121290.
- Waite J. H., Lewis W. S., Magee B. A., Lunine J. I., McKinnon W. B., Glein C. R., Mousis O., Young D. T., Brockwell T., Westlake J., Nguyen M.-J., Teolis B. D., Niemann H. B., McNutt R. L., Perry M., and Ip W.-H. (2009) Liquid water on Enceladus from observations of ammonia and <sup>40</sup>Ar in the plume. *Nature*, 460(7254), 487–490, DOI: 10.1038/nature08153.
- Waite J. H., Glein C. R., Perryman R. S., Teolis B. D., Magee B. A., Miller G., Grimes J., Perry M. E., Miller K. E., Bouquet A., Lunine J. I., Brockwell T., and Bolton S. J. (2017) Cassini finds molecular hydrogen in the Enceladus plume: Evidence for hydrothermal processes. *Science*, 356(6334), 155–159, DOI: 10.1126/science.aai8703.
- Waite J. H., Perryman R. S., Perry M. E., Miller K. E., Bell J., Cravens T. E., Glein C. R., Grimes J., Hedman M., Cuzzi J., Brockwell T., Teolis B., Moore L., Mitchell D. G., Persoon A., Kurth W. S., Wahlund J.-E., Morooka M., Hadid L. Z., Chocron S., Walker J., Nagy A., Yelle R., Ledvina S., Johnson R., Tseng W., Tucker O. J., and Ip W.-H. (2018) Chemical interactions between Saturn's atmosphere and its rings. *Science*, 362(6410), eaat2382.
- Walsh K. J., Morbidelli A., Raymond S. N., O'Brien D. P., and Mandell A. M. (2011) A low mass for Mars from Jupiter's early gas-driven migration. *Nature*, 475, 206–209, DOI: 10.1038/nature10201.
- Watson S. W., Novitsky T. J., Quinby H. L., and Valois F. W. (1977) Determination of bacterial number and biomass in the marine environment. *Appl. Environ. Microbiol.*, 33(4), 940–946.
- Whitman W. B., Coleman D. C., and Wiebe W. J. (1998) Prokaryotes: The unseen majority. *Proc. Natl. Acad. Sci. USA*, 95, 6578–6583.
- Worth R. J., Sigurdsson S., and House C. H. (2013) Seeding life on the moons of the outer planets via Lithopanspermia. *Astrobiology*, 13, 1155–1165, 10.1089/ast.2013.1028.
- Ye S.-Y., Gurnett D. A., Kurth W. S., Averkamp T. F., Kempf S., Hsu H.-W., Srama R., and Grün E. (2014) Properties of dust particles near Saturn inferred from voltage pulses induced by dust impacts on Cassini spacecraft. *J. Geophys. Res.—Space Physics*, 119(8), 6294–6312.
- Yeoh S. K., Li Z., Goldstein D. B., Varghese P. L., Levin D. A., and Trafton L. M. (2017) Constraining the Enceladus plume using numerical simulation and Cassini data. *Icarus*, 281, 357–378.
- Yomogida K. and Matsui T. (1983) Physical properties of ordinary chondrites. *J. Geophys. Res.—Solid Earth*, 88(B11), 9513–9533, DOI: 10.1029/JB088iB11p09513.
- Zhang K. and Nimmo F. (2009) Recent orbital evolution and the internal structures of Enceladus and Dione. *Icarus*, 204(2), 597–609, DOI: 10.1016/j.icarus.2009.07.007.
- Zolotov M. Yu. (2007) An oceanic composition on early and today's Enceladus. *Geophys. Res. Lett.*, 34, L23203, DOI: 10.1029/2007GL031234.
- Zolotov M. Yu. and Kargel J. S. (2009) On the chemical composition of Europa's icy shell, ocean, and underlying rocks. In *Europa* (R. T. Pappalardo et al., eds.), pp. 431–458. Univ. of Arizona, Tucson.